6-16-2018

# Characterization of Mg-based Bimetal Treatment of Insensitive Munition 2,4-dinitroanisole

Emese Hadnagy
*University of New Haven*, ehadnagy@newhaven.edu

Andrew Mai
*Stevens Institute of Technology*

Benjamin Smolinski
*United States Army*

Washington Braida
*Stevens Institute of Technology*

Agamemnon Koutsospyros
*University of New Haven*, akoutsospyros@newhaven.edu



## Publisher Citation

Hadnagy, E., Mai, A., Smolinski, B., Braida, W., & Koutsospyros, A. (2018). Characterization of Mg-based bimetal treatment of insensitive munition 2,4-dinitroanisole. Environmental Science and Pollution Research, 1-14.

## Comments

This is the authors' accepted manuscript of the article published in *Environmental Science and Pollution Research.* The article of record can be found at http://dx.doi.org/10.1007/s11356-018-2493-1.

# Characterization of Mg-based Bimetal Treatment of Insensitive Munition 2,4-dinitroanisole

Emese Hadnagy[1,*], Andrew Mai[2], Benjamin Smolinski[3], Washington Braida[2], Agamemnon Koutsospyros[1]

[*]Corresponding Author. *Email address:* EHadnagy@newhaven.edu
[1]Department of Civil and Environmental Engineering, University of New Haven
[2]Department of Civil, Environmental, and Ocean Engineering, Stevens Institute of Technology
[3]RDECOM-ARDEC

**Abstract**

The manufacturing of insensitive munition 2,4-dinitroanisole (DNAN) generates waste streams that require treatment. DNAN has been treated previously with zero-valent iron (ZVI) and Fe-based bimetals. Use of Mg-based bimetals offers certain advantages including potential higher reactivity and relative insensitivity to pH conditions. This work reports preliminary findings of DNAN degradation by three Mg-based bimetals: Mg/Cu, Mg/Ni, and Mg/Zn. Treatment of DNAN by all three bimetals is highly effective in aqueous solutions (>89% removal) and wastewater (>91% removal) in comparison to treatment solely with zero-valent magnesium (ZVMg; 35% removal). Investigation of reaction byproducts supports a partial degradation pathway involving reduction of the ortho or para nitro- to amino- group, leading to 2-amino-4-nitroanisole (2-ANAN) and 4-amino-2-nitroanisole (4-ANAN). Further reduction of the second nitro group leads to 2, 4-diaminoanisole (DAAN). These byproducts are detected in small quantities in the aqueous phase. Carbon mass balance analysis suggests near complete closure (91%) with 12.4% and 78.4% of the total organic carbon (TOC) distributed in the aqueous and mineral bimetal phases, respectively. Post treatment surface mineral phase analysis indicates $Mg(OH)_2$ as the main oxidized species; oxide formation does not appear to impair treatment.

Keywords: bimetal, magnesium, insensitive munition, reduction, DNAN, wastewater

## 1. Introduction

The quest for safe munitions has led to the development of new formulations, designated as insensitive munitions (IMs), based on components that are less prone to accidental detonation. Manufacturing and handling of these IMs generate waste streams containing mixtures of IMs and their manufacturing and transformation byproducts that require further treatment. One specific IM component, 2,4-dinitroanisole (DNAN) has seen heavy use, and thus has garnered research interests in different treatment methods to degrade this target compound in waste streams.

Degradation of pure DNAN by ZVI (Hawari *et al.*, 2015) and its photodegradation (Rao *et al.*, 2013a; Arthur *et al.*, 2017) have been reported. In addition, extensive research on the degradation of DNAN in IM wastewater has been conducted. These studies have evaluated various technologies including: phytoremediation (Shih *et al.*, 2009), aerobic biodegradation (Fida *et al.*, 2014), ZVI/Fenton treatment (Liu *et al.*, 2015), ZVI/anaerobic digestion (Ahn *et al.*, 2011), Fe/Cu bimetal/Fenton treatment (Shen *et al.*, 2013), and reduction by Fe/Cu (Koutsospyros *et al.*, 2012; Kitcher *et al.*, 2017). Treatment of DNAN by bimetals typically exhibits several advantages when compared to other technologies including extremely rapid degradation kinetics leading to high removal efficiency. DNAN degradation with Fe-based bimetals exhibited fast degradation with complete removal in several minutes (Kitcher *et al.*, 2017). Although treatment of DNAN with Fe-based reagents (ZVI or bimetals) has been demonstrated, the potential use of a similar reagent (i.e. Mg-based bimetals) has not yet been explored.

The bimetal technology is based on enhancing the reactivity of a zero-valent base metal by close contact (i.e. coating) with a catalytic metal to create a galvanic cell. Both Mg and ZVI have been combined with various catalytic metals to produce reductive bimetal systems that have

treated effectively halogenated compounds and nitro-based explosives (Morales *et al.*, 2002; DeVor *et al.*, 2009; Begum and Gautam, 2011; Koutsospyros *et al.*, 2012; Liu *et al.*, 2015). Specifically, Mg-based bimetals are an emerging technology for the treatment of various organic (Gautam and Suresh, 2007; DeVor *et al.*, 2008; Agarwal, Al-Abed and Dionysiou, 2009; Ghauch and Tuqan, 2009) and inorganic contaminants (Ramavandi *et al.*, 2011). Magnesium has attracted additional interest due to its greater electrode potential than iron. In the hydrogenation of phenol to cyclohexane and cyclohexanone, Mg/Pd was found more effective than Fe/Pd, and $Mg^0$ was more effective than $Fe^0$ (Morales *et al.*, 2002). In addition to the selection of a base metal, the choice of catalytic metal can improve treatment effectiveness by increasing the galvanic potential difference between the pair. Some researchers have utilized noble metals to increase the galvanic potential difference such as Pd, Ag, and Au (Cwiertny *et al.*, 2006; DeVor *et al.*, 2008; Patel and Suresh, 2008; Coutts *et al.*, 2011; Saitta *et al.*, 2015). Catalytic metal selection criteria may be expanded to include economic (e.g. cost), sustainability (e.g. relative abundance, available deposits) and environmental (e.g. regulatory levels) considerations. In this respect, other more inexpensive and readily available metals, such as Cu, Ni, and Zn may be attractive alternatives for use in bimetal formulations.

Similar to many other organic compounds, treatment of DNAN by chemical or biological methods may generate transformation byproducts. Identification of byproducts is critical for unveiling the contaminant degradation pathway and establishing that transformed products are toxicologically and environmentally more benign than the parent contaminant. Treatment methods such as photodegradation (Rao *et al.*, 2013b; Hawari *et al.*, 2015; Taylor *et al.*, 2017) and aerobic biodegradation (Fida *et al.*, 2014; Karthikeyan and Spain, 2016) are typically oxidative. Conversely, typical transformation pathways in treatment with ZVI, ZVMg or Fe- and

Mg-based bimetals indicate reductive chemistry, as observed for example in the reduction of nitrate to nitrite (Ileri, Ayyildiz and Apaydin, 2015; Khalil *et al.*, 2016), Cr(VI) to Cr(III) (Rivero-Huguet and Marshall, 2009), and the reductive dechlorination of PCBs (Hadnagy, Rauch and Gardner, 2007; Agarwal *et al.*, 2009; Coutts *et al.*, 2011). Reduction of nitro groups by ZVI or Fe-bimetals in various energetics has been demonstrated in the literature. Examples include treatment of 1,3,5-trinitroperhydro-1,3,5-triazine (RDX) by Fe/Cu (Koutsospyros *et al.*, 2012), dinitrophenol (DNP) and dinitrochlorobenzene (DNCB) by Fe/Cu (Liu *et al.*, 2015) and DNAN by ZVI and Fe/Cu (Ahn *et al.*, 2011; Hawari *et al.*, 2015; Kitcher *et al.*, 2017).

In the present work, reductive degradation of DNAN is reported using Mg-based bimetals containing relatively inexpensive and readily available secondary (i.e. catalytic) metals. Three bimetal formulations are evaluated, namely Mg/Cu, Mg/Ni, and Mg/Zn and are compared to degradation with ZVMg. The treatment process is evaluated in laboratory prepared DNAN aqueous solutions and in wastewater. Additionally, SEM imaging, EDS, and XRD analyses are used for characterization of the bimetal reagent surface of unused and used particles (i.e. before and after treatment). Furthermore, identification and quantification of byproducts in the dissolved and particulate phases are performed to facilitate carbon mass balance analysis.

## 2. Methods

### *2.1 Chemicals and Materials*

Solid magnesium particles (20-230 mesh, reagent grade, 98% purity), nickel(II) chloride (98% purity), zinc chloride (98% purity) and glacial acetic acid (99%+) were purchased from Sigma Aldrich (St. Louis, MO). Copper(II) chloride (99%), acetonitrile (99.5%, ACS grade), glass fiber filter paper (<1 micron, 55 mm) and nylon filter paper (0.45 micron, 55 mm) were purchased from Fisher Scientific (Waltham, MA). Syringe filters (0.45 micron, nylon) were purchased from Achemtek (Worcester, MA). DNAN solids and DNAN, RDX, and NQ (nitroguanidine) standards dissolved in acetonitrile were obtained from Picatinny Arsenal (Wharton, NJ). DNP standard dissolved in methanol, DAAN (2,4-diaminoanisole*)* solid standard, and 2-ANAN (2-amino-4-nitro-anisole*,* 98%) were purchased from Sigma Aldrich (St. Louis, MO) and 4-ANAN (2-nitro-4-amino-anisole*,* 97%) was purchased from Fisher Scientific. TOC standards were purchased from Fisher Scientific (Waltham, MA). Chemical oxygen demand (COD) kits (TNT 821) and total nitrogen (TN) kits (TNT 826) were purchased from Hach (Loveland, CO). Photometric analyses using these test kits were performed on a HACH spectrophotometer DR 6000 (Loveland, CO).

The composition of the IM wastewater, obtained from an industrial munitions facility, is reported in Table 1. In addition to DNAN, RDX, NQ, and DNP were also identified and quantified in the wastewater. Additional wastewater characterization included pH, inorganic nitrogen species ($NH_3$, $NO_2$, $NO_3$), TN, COD and TOC. Information on wastewater composition is provided for completeness of information. The target compound for the present work is only DNAN.

**Table 1.** DNAN Wastewater Characteristics[1]

| RDX (mg $L^{-1}$) | NQ (mg $L^{-1}$) | DNAN (mg $L^{-1}$) | DNP (mg $L^{-1}$) | pH | $NH_3$-N (mg $L^{-1}$) | $NO_2$-N (mg $L^{-1}$) | $NO_3$-N (mg $L^{-1}$) | TN (mg $L^{-1}$) | COD (mg $L^{-1}$) | TOC (mg $L^{-1}$) |
|---|---|---|---|---|---|---|---|---|---|---|
| 5 | 0.5 | 110 | 150 | 7.08 | B.D.L. | B.D.L. | 3.08 | 47 | 470 | 120 |

[1] B.D.L. = below detection limit

*2.2 Treatment Experiments*

Completely mixed laboratory batch experiments were conducted to evaluate the efficacy of DNAN treatment using select Mg-based bimetals. All experiments were carried out in 40 mL VOA vials using a 22 mL reaction volume at 0.5 % solids/liquid (S/L) ratio and 10:1 Mg to secondary metal (i.e. Cu, Ni, Zn) ratio. Additional experiments for byproducts and mass balance used different reaction volumes (15-132 mL) with the same S/L ratio and all other identical conditions. The 0.5% S/L ratio was chosen based on previously reported work on DNAN degradation using Fe-based bimetals (Koutsospyros *et al.*, 2012). The 10:1 Mg to secondary metal ratio was decided based on several other studies using Mg in bimetal formulations. Mg/Cu was used in 10:1 ratio to treat azo dye (Asgari, Ramavandi and Farjadfard, 2013), and endosulfan and lindane were treated with Mg/Pd at 7.5:1 and 5:1 ratios (Begum and Gautam, 2011) and at 50:1 ratio (Aginhotri, Mahidrakar and Gautam, 2011). In the present study, 0.11 g of Mg granules, 10 mL of water and 1 mL of catalytic metal solution (22.27, 24.29, 22.94 g/L for $CuCl_2$, $NiCl_2$, and $ZnCl_2$, respectively) prepared in deionized water were combined and mixed on a magnetic stirrer plate (Color Squid model, IKA, Wilmington, NC) at a mixing speed of 500 rpm for 5 min. In experiments with ZVMg, the volume of catalytic metal was replaced with additional DI water. The treatment was initiated by adding 10 mL of DNAN wastewater or a 250 mg $L^{-1}$ pure DNAN aqueous solution. After 2.5 h treatment, an aliquot of the dissolved phase was analyzed by filtering the mixture with a nylon syringe filter (0.45 micron, Achemtek).

131 *2.2.1. Mass Balance Experiments*

132 Mass balance experiments were performed to measure dissolved, adsorbed and volatilized TOC
133 and were carried out under identical treatment conditions (aqueous solutions, 0.5% S/L, 2.5 hr
134 treatment time, and 10:1 Mg to catalytic metal ratio). However, dissolved TOC measurements
135 were performed in experiments scaled by 3 (i.e. 66 mL total rather than 22 mL in previous
136 experiments). Adsorbed TOC was measured indirectly by acid digestion of the entire reaction
137 mixture (i.e. treated solution and bimetal together). Therefore, the TOC adsorbed to the bimetal
138 could be determined by subtracting the dissolved TOC from the combined adsorbed and
139 dissolved TOC measurements. Acid digestions were performed by the addition of 1 mL of
140 sulfuric acid (technical grade, 95% purity). Additionally, experiments for adsorbed TOC
141 measurements used an adjusted synthesis step that used less water (i.e. 5 mL instead of the
142 previous 11 mL). Volatilized TOC were analyzed qualitatively by GC-MS by capturing the gas
143 in multilayer foil gas bags (Supelco, Bellefonte, PA), however gaseous species were not
144 detected.

145 *2.3 Analytical Methods*

146 DNAN was analyzed by reversed phase high pressure liquid chromatography (HPLC) on an
147 Agilent 1260 HPLC instrument (Santa Clara, CA) equipped with a Grace Alltech Adsorbosphere
148 HS C-18 (5µm, 250x4.6mm) and a DAD detector (i.e. HPLC-DAD). The mobile phase was an
149 isocratic mixture of methanol:water at 70:30 (v/v), pumped at 1 mL $min^{-1}$; the injection volume
150 was 30 µL of sample; the analytical wavelength was 300 nm (optimal absorbance wavelength for
151 DNAN). At these conditions, DNAN eluted at 4.1 min.

152 Quantification of 2,4-dinitrophenol (DNP) on HPLC was based on an isocratic flow using
153 a solvent of 20% methanol and 80% water at a flow rate of 1 mL $min^{-1}$; DNP eluted at 2.5 min.

Simultaneous measurements of DNAN, 2-ANAN, 4-ANAN and DAAN were performed on the same column and detector. A separate analytical method was developed for this analysis, which used a 5 min hold of 90:10 water-methanol mobile phase, followed by a 50 min gradient to 10% water, 90% methanol and with a 5 min hold of 10% water, 90% methanol pumped at a flow rate of 1 mL $min^{-1}$. At these conditions, the elution times were: DAAN at 5.5 min, 4-ANAN at 19 min, 2-ANAN at 26 min, and DNAN at 32 min. The analytical wavelength used was 254 nm (a wavelength at which all four compounds of interest absorb well). The gradient method was used due to greatly different hydrophobicity and, therefore, significantly different retention times of DAAN and DNAN.

TOC was measured via a UV-Persulfate TOC Analyzer Phoenix 8000 instrument from Teledyne Tekmar (Mason, OH). Identification of byproducts was performed using electrospray ionization tandem mass spectrometry (ESI-MS/MS) on a Waters Quattro Ultima (Milford, MA), i.e. through direct injection of the sample without any separation. Analyses were performed in both positive and negative ionization modes. Tandem mass spectrometry (MS/MS) was essential due to the injection of mixtures (e.g. treated pure compound generating several byproducts) and also in acquiring the necessary daughter spectra for compound identification. ESI-MS, combined with front-end separation with HPLC (i.e. HPLC-ESI-MS), was used for additional confirmation (HPLC: Agilent 1100 Series, Santa Clara, CA; MS: Waters Micromass ZQ instrument, Milford, MA).

*2.4 Surface Characterization*

XRD patterns were acquired on a Rigaku Ultima IV X-Ray diffractometer (The Woodlands, TX). Scans acquired were from 5 to 65 2θ with an increment of 0.03 θ and scan speed of 2 seconds. The x-ray conditions were 40 kV and 40 mA. These were the recommended standard

177 method and conditions according to the manufacturer. SEM images were obtained with focus ion
178 beam scanning electron microscopy (FIB-SEM), and EDS analyses were performed with a
179 silicon drift detector (SDD) both on a Zeiss Auriga instrument (Oberkochen, Germany).
180 The surface of the bimetals was examined by SEM, XRD, and EDS analyses both before and
181 after treatment, referred to as unused and used particles, respectively. One sample for each
182 bimetal (i.e. Mg/Cu, Mg/Zn, and Mg/Ni) was prepared. Unused particles were synthesized under
183 the same conditions as used ones except without the addition of DNAN. Treated bimetal solids
184 were separated from the liquid by vacuum filtration and allowed to dry on glass slides for 30-60
185 min. Unused samples were decanted and dried overnight to ensure complete dryness.
186

187 ## 3. Results and Discussion

188 *3.1 Bimetal Synthesis and Characterization*

189 Bimetal particles were synthesized in this work and, therefore, surface characterization
190 was required to ensure that the catalytic metal had coated the base metal. SEM imaging with
191 backscatter detection allowed the detection of the heavier catalytic metals (i.e. Cu, Ni, and Zn),
192 which appeared brighter than the less heavy base metal Mg on the images. For each bimetal
193 configuration, successful coating of the base metal by the catalytic metal was observed. Solid Cu
194 nanoparticles (<100nm) coated the Mg (Figure 1a). A contrasted and zoomed-in image allowed
195 better observation of the bright Cu nanoparticles (Figure S.1). Other studies that evaluated the
196 Mg/Pd bimetal found small islands of Pd deposits (i.e. 50-100 nm) on the Mg surface using the
197 same imaging technique (Agarwal, Al-Abed and Dionysiou, 2007). In the present work, solid Zn
198 was coated on the Mg in the form of larger micron-sized particles (Figure 1b). This figure is
199 presented at smaller magnification in order to optimally view the Zn deposits against the Mg

base metal. In contrast to the Cu and Zn particles, Ni was observed to coat the Mg uniformly, an observation supported by the lack of distinct structures on the surface of the Mg/Ni bimetal (Figure 1c).

**Fig. 1** SEM images of catalytic metal coating on the Mg base metal: (a) Mg/Cu: Cu nanoparticles ('bright spots'), (b) Mg/Zn: micron-sized Zn deposits, and (c) Mg/Ni: uniform Ni coating

*3.2 Degradation of Pure DNAN in the Aqueous Phase*

The degradation of the target compound DNAN was first examined in laboratory-made aqueous solution. This was done to isolate the behavior of the compound from the wastewater matrix. Treatment of aqueous solutions of pure DNAN with any of the three bimetals resulted in significantly higher extent of removal compared to that of ZVMg alone, i.e. without the addition of a catalytic metal (Figure 2). The treatment efficiency of the Mg/Cu, Mg/Zn and Mg/Ni bimetal configurations was 100%, 95% and 89% removal, respectively. ZVMg performed poorly at a removal efficiency of 35%. Poor removal efficiencies of ZVMg and ZVI with systems near neutral pH have been reported for nitrate and Cr(VI) reduction, by Khalil et al. (2016) and Rivero-Huguet et al. (2009). Furthermore, enhancement of reductive degradation by addition of a catalytic salt has been reported for Fe-based bimetals (Rivero-Huguet and Marshall, 2009; Xiong *et al.*, 2015; Khalil *et al.*, 2016) and Mg-based bimetals (Solanki and Murthy, 2011; Saitta *et al.*, 2015) for various inorganic and organic contaminants. In the present work, degradation by ZVMg was evidently similarly enhanced with the addition of the catalytic metal.

**Fig. 2** Pure DNAN removal (%) in the aqueous phase after bimetal treatment (0.5% S/L, 10:1 Mg to catalytic metal ratio, and 2.5 h treatment time) compared to ZVMg treatment

After treatment with ZVMg and the bimetals, the final pH was higher than that of the original DNAN aqueous solution. This was likely due to the consumption of protons ($H^+$) during the chemical reduction (Begum and Gautam, 2011; Khalil *et al.*, 2016). Furthermore, treatment with any of the three bimetals equilibrated to a final pH in the range of 9.9-10.2, while treatment with ZVMg resulted in a higher final pH of 10.7 (Table 2). Reduction of nitrate by ZVI also generated a higher pH than treatment by Fe/Cu (Khalil *et al.*, 2016). Oxidized species of Cu and Fe (i.e. $CuFe_2O_4$*$Fe_3O_4$) had formed, and these side reactions likely generated protons; therefore, the final pH was lower in the Fe/Cu treated system. Similar reactions may have occurred during reduction with ZVMg versus a Mg-bimetal in the present study, i.e. side reactions during the formation of oxidized metal species of the base metal Mg and/or catalytic metal may generate $H^+$ thereby reducing the pH.

**Table 2. Parameters of DNAN Treatment in Two Matrices***

| Matrix | System | Initial pH** | Final pH | Initial ORP** (mV) | Final ORP (mV) | DNAN Removal (%) |
|---|---|---|---|---|---|---|
| | Control | 5.70 (±0.10) | 5.01 (±0.34) | 76 (±44) | 171 (±34) | 1.6 (±0.5) |
| | ZVMg | 9.77 (±0.64) | 10.72 (±0.10) | 82 (±36) | 24 (±8) | 35.1 (±4.0) |
| | Mg/Cu | 9.42 (±0.53) | 10.20 (±0.06) | -96 (±20) | -96 (±12) | 100.0 (±0.0) |
| | Mg/Ni | 7.92 (±0.08) | 9.91 (±0.08) | -16 (±27) | -108 (±22) | 88.8 (±3.6) |
| | Mg/Zn | 7.03 (±0.36) | 10.22 (±0.05) | 27 (±11) | -7 (±7) | 94.7 (±1.6) |
| | Control | 6.64 (±0.01) | 7.15 (±0.09) | 196 (±64) | 199 (±10) | 6.2 (±0.3) |
| | ZVMg | 10.18 (±0.06) | 10.86 (±0.06) | -131 (±20) | 36 (±4) | 12.9 (±2.0) |
| | Mg/Cu | 10.43 (±0.07) | 9.99 (±0.08) | -295 (±37) | -225 (±8) | 100.0 (±0.0) |
| | Mg/Ni | 7.96 (±0.07) | 9.93 (±0.09) | -231 (±27) | -188 (±20) | 97.2 (±0.4) |
| | Mg/Zn | 8.32 (±0.57) | 10.15 (±0.10) | -108 (±55) | -158 (±18) | 90.5 (±3.5) |

*Treatment time of 2.5 h

**Initial pH and initial ORP obtained for treated samples were measurements taken immediately after contact between DNAN and the reagents had been established

*3.3 Reaction Byproduct Identification in the Dissolved Phase*

To shed light to the Mg-based reductive degradation of DNAN, it is critical to identify and quantify the reaction products formed. Mass spectra were acquired from treated samples in both the aqueous solution and wastewater experiments using ESI-MS/MS and HPLC-ESI-MS in positive and negative ionization modes. Detection of products at the attempted initial DNAN concentration was not possible due to low concentrations close to detection levels. Since higher initial DNAN concentrations could not be pursued due to aqueous solubility limitations, experiments were set up using an alternative solvent. Products were, however, identified under different conditions: 1) treatment of pure DNAN in an acetonitrile solvent matrix and 2) treatment of an identified byproduct, 4-ANAN, in DI water. Products were characterized only for Mg/Cu treatment.

*3.3.1 DNAN Treated in a Solvent Matrix*

A solvent matrix (i.e. ACN) was used to produce higher initial DNAN concentrations, which led to higher, detectable concentrations of byproducts. Treatment conditions were identical to those of previously mentioned experiments (i.e. 0.5% S/L ratio, 10:1 Mg to Cu ratio) except that the initial stock solution contained 1,350 mg $L^{-1}$ DNAN in ACN as opposed to the earlier 250 mg $L^{-1}$ DNAN in water. In ACN, the daughter spectrum of m/z 169 in positive ionization mode produced fragmentation that indicated the production of 2-ANAN and 4-ANAN during treatment (Figure 3a). The daughter spectrum of m/z 139 produced fragmentation that indicated the formation of DAAN (Figure S.2a). Reference spectra were acquired from aqueous solutions of 2-ANAN, 4-ANAN (Figure 3b, c) and DAAN (Figure S.2b) to confirm their presence in the treated DNAN sample. The peaks at m/z 169 for the 2-ANAN and 4-ANAN spectra and at m/z 139 for the DAAN spectrum were identified as the protonated species, i.e. $[M+H]^+$, because the nominal masses of the neutral molecules are 168 and 138 Da, respectively. In negative ionization mode,

no other significant peaks, other than those corresponding to 2-ANAN, 4-ANAN or DAAN, were observed.

**Fig. 3** Daughter spectrum of m/z 169 from ESI-MS/MS in positive mode from (a) after DNAN treatment (solvent matrix, 0.5% S/L, 10:1 Mg to Cu ratio, 2.5 hour treatment time), (b) pure 2-ANAN reference, and (c) pure 4-ANAN reference. The difference in maximum intensities are neglected as comparison of relative intensities were required

DAAN was also detected when DNAN was reduced with ZVI by Hawari et al. (2015) and Ahn et al. (2011) and with Fe/Cu by Liu et al., 2015 (Ahn *et al.*, 2011; Hawari *et al.*, 2015; Liu *et al.*, 2015). Ahn et al. (2011) also identified both 2-ANAN and 4-ANAN similarly to the present work (Ahn *et al.*, 2011), while Hawari et al. (2015) only detected 2-ANAN as byproducts of DNAN degradation. Hawari et al. (2015) attributed the fact that only 2-ANAN was detected in their study to the regioselectivity of reduction in the ortho position, i.e. reduction more favorably produced 2-ANAN over 4-ANAN; therefore, 4-ANAN generated was below the detection limit (Hawari *et al.*, 2015). Kitcher et al. (2017) confirmed reduction of nitro groups to amino groups by in source deuterium exchange, which indicated m/z 169 as an amino product; it was assumed that m/z 169 meant both ortho and para reduction occurred, i.e. both 2-ANAN and 4-ANAN were formed (Kitcher *et al.*, 2017).

In the present study, the analysis of daughter spectra revealed that 2-ANAN produced mass spectral peaks of m/z (in positive mode): 169, 154, and 123. 4-ANAN produced mass spectral peaks of m/z: 169, 154, 152, 123, 122, and 94. The low intensity of m/z 152 in the treated sample (Figure 3a) indicates that a mixture of both 4-ANAN and 2-ANAN was present. For example, if only 4-ANAN were present, the intensity of m/z 152 peak would be higher,

289 while if only 2-ANAN were present, there would be no peak at m/z 152. However, there is a
290 minute peak of m/z 152 in the mass spectrum (Figure 3a). In addition, the same was observed
291 with the relative intensity of the m/z 123 and 122 peaks. If only 4-ANAN were present, the m/z
292 122 peak in Figure 3a would be relatively higher to that of m/z 123, i.e. the two peaks should
293 match the relative heights of the m/z 122 and 123 peaks in the 4-ANAN reference. Ultimately,
294 the presence of 2-ANAN effectively suppressed the intensity of the m/z 122 peak when mixed
295 with 4-ANAN. Olivares et al. (2016) was also able to differentiate between the 2-ANAN and 4-
296 ANAN isomers based on their unique fragmentation patterns. Furthermore, Hawari et al. (2015)
297 detected a hydroxylamino intermediate (i.e. 2-HA-NAN) and small amounts of a nitroso
298 intermediate (i.e. 2-NO-NAN). According to Hudlicky (1984), reduction of the nitro group in
299 nitroaromatic compounds follows the scheme: nitro ($-NO_2$) > nitroso (-NO) > hydroxylamino (-
300 NHOH) > amine ($-NH_2$), according to the degree of reduction. Nitroso and hydroxylamino
301 compounds are typically rarely observed under this scheme (Hudlicky, 1984). In this study, no
302 nitroso or hydroxylamino intermediates in either the ortho or para positions were identified.

303 *3.3.2 Reduction of 4-ANAN to DAAN*

304 The high aqueous solubility of 4-ANAN (4,400 mg $L^{-1}$ at 25°C (Hawari *et al.*, 2015)), an
305 identified byproduct of DNAN degradation in the ACN matrix, allowed investigation of further
306 byproduct formation directly in aqueous solutions, i.e. as opposed to work performed in an ACN
307 matrix. The reduction of 4-ANAN to DAAN was confirmed; treatment of 4-ANAN (800 mg $L^{-1}$
308 initial concentration, 0.5% S/L, 10:1 Mg to Cu ratio, 1 hour treatment time) yielded DAAN (m/z
309 139) (Figure 4). The presence of DAAN was additionally confirmed on HPLC-ESI-MS for the
310 same treatment condition (Figure S.3). Adding front-end separation with HPLC to the MS
311 method allowed the matching of elution times of pure DAAN (observed as m/z 139) to that of

312 the m/z 139 peak in treated 4-ANAN. Although the reduction of 4-ANAN to DAAN has been
313 proposed as part of the DNAN degradation pathway using ZVI (Ahn *et al.*, 2011; Hawari *et al.*,
314 2015) and Fe/Cu (Kitcher *et al.*, 2017), the same has not yet been reported for Mg-based bimetal
315 treatment in the literature. Additionally, the detection of DNAN reduction to DAAN by any
316 bimetal has not yet reported until now; Kitcher et al. (2017) proposed DAAN as a probable final
317 product by Fe-bimetal reduction, but could not confirm analytically.
318
319 **Fig. 4** Daughter spectrum of m/z 139 from ESI-MS/MS in positive mode of 4-ANAN treated
320 with Mg/Cu (DI water matrix, 0.5% S/L, 10:1 Mg to Cu ratio, 1 hr treatment time) showing
321 DAAN (m/z 139) with matching fragmentation of pure DAAN (Figure S.2b)
322
323 *3.4 Reaction Pathway*
324 The proposed partial reaction pathway for DNAN reduction by Mg/Cu is: 1) reduction of
325 one nitro group, either ortho or meta position, which forms 2-ANAN or 4-ANAN, and then 2)
326 subsequent reduction of the other nitro group, which forms DAAN (Figure 5). This pathway was
327 identical to the one identified for DNAN reduction with ZVI (Ahn *et al.*, 2011) and Fe/Cu
328 (Kitcher *et al.*, 2017). In the present study, the byproducts and reaction pathways characterized
329 to-date were from DNAN treatment with Mg/Cu, and it is likely that identical pathways exist for
330 treatment with Mg/Ni and Mg/Zn. The proposed pathway excludes the unstable nitroso and
331 hydroxylamine derivatives discussed earlier since these compounds were not detected.
332
333 **Fig. 5** Partial reaction pathways of DNAN degradation by Mg/Cu
334

335 The reduction of DNAN to byproducts 2-ANAN, 4-ANAN and DAAN were made possible by
336 electrons released by the dissolution of $Mg^0$ as illustrated in Figure 6. In the bimetal pair, Mg/Cu,
337 Cu is the cathode while Mg is the anode. Mg thus preferentially corrodes to $Mg^{2+}$ with the
338 concurrent release of 2 electrons. Electrons become available for reduction illustrated by the
339 dashed lines. In addition, $Mg(OH)_2$ forms by the oxidation of Mg in water (Figure 6). The same
340 reactions occur in the case of Mg/Ni and Mg/Zn, where Ni and Zn are cathodic relative to the
341 Mg.
342
343 **Fig. 6** Diagram illustrating the galvanic corrosion of Mg in the Mg/Cu bimetal pair resulting in
344 reduction of DNAN and oxidation of Mg to $Mg(OH)_2$
345
346 *3.5 Quantification of Reaction Byproducts and Mass Balance*
347 Mass balance experiments are necessary in order to fully characterize any treatment
348 system. A significantly open mass balance means undetected compounds or unknown fates, with
349 potential to toxic exposure. In the present study, preliminary mass balance data were obtained for
350 treatment of pure DNAN in water and in ACN with Mg/Cu. Since byproducts of pure DNAN
351 were not detected in the aqueous (i.e. dissolved) phase, the TOC mass balance was evaluated
352 (see Section 3.5.1). Next, experiments with pure DNAN were performed in ACN and the mass
353 balance of DNAN and its known reaction products was evaluated in the combined dissolved and
354 adsorbed phase (obtained by acid digestion of the reaction mixture), with subsequent
355 quantification of individual known compounds in the dissolved phase (see Section 3.5.2).
356 *3.5.1 Overall Carbon Mass Balance Closure Using Aggregate TOC Measurements*

After treatment of pure DNAN with Mg/Cu, a 91% carbon mass balance closure was attained by addition of the dissolved and adsorbed phases (i.e. adsorbed to the bimetal surface). The dissolved phase and adsorbed phase contained 12.4% and 78.4% of TOC, respectively, compared to the control. On the other hand, treatment of DNAN by ZVI resulted in 95% of the initial DNAN mass recovered as DAAN in the aqueous phase after 1 hour of treatment (Ahn *et al.*, 2011). This observed difference of mass balance between ZVI in the study of Ahn et al. (2011) and Mg/Cu in the present work might stem from increased oxidization of the Mg-bimetal from galvanic corrosion. The enhanced corrosion of the Mg surface during treatment may have increased the total surface area and therefore increased the number of sites available for adsorption.

This significant adsorption was validated by analysis of the sealed reactor headspace with GC-MS in experiments conducted with aqueous solutions of pure DNAN. A significant amount of gas (approximately 0.5-1.0L) was generated (with reaction volumes of 132 mL), but no reaction byproducts were identified. The gas captured was speculated to be mainly $H_2$ gas, an expected gas formed in the dissolution of Mg or Fe in water (Patel and Suresh, 2007; Lee and Park, 2013; Nie *et al.*, 2013).

*3.5.2 Mass Balance of Dissolved Byproducts: Treatment in Solvent Matrix*

Byproducts in the dissolved phase have been qualitatively detected. However, quantification of dissolved byproducts was necessary to close the mass balance in the liquid phase to ensure that the products detected (2-ANAN, 4-ANAN and DAAN) accounted for all dissolved TOC. Significant open mass balance in the liquid phase would indicate formation of additional unidentified products. Byproducts in the dissolved phase after DNAN treatment in aqueous solutions could not be detected by MS or HPLC. However, byproducts 2-ANAN and 4-ANAN

were detected in small amounts for DNAN treatment by Mg/Cu in ACN (Figure 7). Furthermore, dissolved DAAN was detected on ESI-MS, but was not detected on the HPLC-DAD used for quantification, and therefore the bar for DAAN was marked with an asterisk (*) to indicate future work is needed for analytical method development for this compound. Mass balance data from aggregate measurements after treatment in the solvent matrix could not be supplemented with COD and TOC removals due to the significant addition of ACN. Ultimately, the small amounts of 2-ANAN and 4-ANAN found after treatment in the ACN matrix and the undetectable amounts of the same compounds in the aqueous matrix could indicate that DAAN may further degrade to other compounds. Furthermore, the higher concentration of 2-ANAN than that of 4-ANAN on Figure 7 maybe suggestive of regioselectivity of the reduction reaction for the ortho rather than the para isomer. This remains to be resolved and quantified in future work.

**Fig. 7** Recovered mass of DNAN and products in the dissolved phase after treatment of DNAN with Mg/Cu (ACN matrix, 0.5% S/L, 10:1 Mg to Cu ratio, 2.5 hr treatment). Zero amounts of DAAN marked with (*) indicate quantification of this compound requires additional work. Corresponding chromatogram of treated DNAN in upper right; DAAN was not detected on HPLC-DAD

397 *3.6 Characterization of DNAN Treatment in Wastewater*

398 Parameters examined for DNAN-laden wastewater treatment included DNAN removal,
399 pH, ORP, TOC and COD reduction, and removal of dinitrophenol (DNP) (DNP was only
400 evaluated qualitatively), another major wastewater constituent. Observed DNAN removals in
401 wastewater were similar to those of in the pure DNAN solutions. In the wastewater, high
402 removals were achieved by Mg/Cu, Mg/Ni, and Mg/Zn (i.e. 100%, 97% and 91%, respectively),
403 while treatment with ZVMg resulted in poor degradation efficiency of 12.9% (Figure 8).
404 However, treatment with Mg/Zn resulted in lower DNAN removal than treatment with Mg/Ni in
405 wastewater, whereas the opposite trend was observed in aqueous solutions (Table 2).
406
407 **Fig. 8** DNAN removal (%) in wastewater after bimetal treatment (0.5% S/L, 10:1 Mg to catalytic
408 metal ratio, and 2.5 h treatment time) compared to ZVMg
409
410 Based on removal efficiency, the reductive activity of the various bimetal systems was
411 ranked in the following order (treatment of aqueous solutions of pure DNAN):
412 Mg/Cu>Mg/Zn>Mg/Ni>ZVMg (Table 2). There was no correlation between the final ORP
413 values and the DNAN removal efficiencies. On the other hand, a correlation has been observed
414 between these variables for wastewater experiments. In the wastewater matrix, the final ORP
415 values showed that the Mg/Cu bimetal pair exhibited the most negative value (-225 mV),
416 indicating that this system generated the most reductive environment. Based on ORP values, the
417 bimetal systems were ranked in the following order (most negative shown first):
418 Mg/Cu<Mg/Ni<Mg/Zn<ZVMg, which correlated with the DNAN removal efficiency (i.e. higher
419 DNAN removal was achieved under more reducing conditions). The reduction of nitrate by ZVI

and Fe/Cu also created a reductive environment as indicated by negative ORP values of around -700 mV (Khalil *et al.*, 2016); the difference in ORP values between reduction with ZVI and Fe/Cu was not significantly different. Final pH values in wastewater were similar to those observed in pure DNAN aqueous solutions: pH of 9.9-10.2 for the bimetals and somewhat higher pH of 10.9 for ZVMg (Table 2).

*3.7 Removal of TOC and COD*

The effectiveness of wastewater treatment using bimetals was also measured by removal of aggregate parameters TOC and COD. Aggregate parameters were selected because although the major constituents were DNAN, DNP, and RDX, small amounts of other unknown compounds accounted for approximately 10% of wastewater TOC.

All three bimetal systems were capable of high DNAN removal of 90-100% (Figure 8) and TOC and COD removal of 60-70% (Figure S.4). Empirical measurements of TOC and COD from solutions of DNAN at various concentrations allowed calculation of DNAN-derived TOC and COD. The majority of the remaining TOC and COD after treatment were, therefore, DNAN byproducts and/or byproducts derived from DNP and RDX. In addition, the overall amount of removed TOC and COD exceeded that originating from DNAN. Therefore, the system treated the other organic contaminants as well as DNAN. The remaining TOC and COD may also include species that were more resistant to the bimetal treatment. This was corroborated by a similar level of TOC and COD removal regardless of bimetal configuration and despite the larger DNAN removal capability of Mg/Cu. COD removal was not measured for treatment with ZVMg.

Furthermore, the degradation of DNP by Mg/Cu, Mg/Ni and Mg/Zn, was qualitatively observed by superimposing HPLC chromatograms of wastewater at before and after treatment

444 (0.5% S/L, 10:1 Mg to catalytic metal ratio) (Figure S.5). The intensity of the chromatographic
445 peak that correlated to DNP (2.1 min) decreased drastically indicating almost complete removal
446 after treatment with each bimetal. The same result was observed for DNAN (4.2 min).
447
448 *3.8 Effect of Treatment on the Bimetal Surface*
449 The characterization of the reagent bimetal surface after use was performed to assess any
450 changes to the reagent. For bimetal systems and especially Fe-based bimetals, oxidation of the
451 bimetal surface has led to passivation and inhibition of treatment (Rivero-Huguet and Marshall,
452 2009; Fu, Cheng and Lu, 2015; Sun *et al.*, 2016). In this work, surface analyses of used Mg-
453 bimetal particles included SEM imaging, elemental mapping through EDS, and XRD analysis.
454 EDS results indicated significant elemental oxygen on the surface of all tested bimetal
455 configurations. Therefore, the identification and relative quantification of the mineral species
456 containing oxygen was performed by XRD analysis.
457 *3.8.1 Elemental Analyses of Oxidation with EDS*
458 The EDS map of an unused particle of Mg/Cu (Figure 9) showed that oxygen was distributed
459 according to the topography of the Mg surface, which suggested oxidation of the Mg surface
460 (Figure 9b, c). Therefore, the surface of Mg/Cu particles had become oxidized during the bimetal
461 synthesis step before treatment. Oxidation of the surface was likely due to galvanic corrosion
462 after deposition of $Cu^0$. The Cu nanoparticles were not clearly detectable on EDS mapping
463 (Figure 9d) but were observed on SEM imaging (Figure 1a).
464
465 **Fig. 9** EDS mapping of (a) a sample region of an unused Mg/Cu particle pictured by SEM of an
466 elucidating distribution of (b) primary metal Mg to (c) oxygen, (d) and catalytic metal Cu

After treatment (i.e. on used particles), identification of Cu nanoparticles on SEM images and EDS mapping was not as certain due to the 'rougher' particle appearance resulting from corrosion (Figure 10a). However, EDS elemental analysis still showed the presence of Cu on the treated particle (Figure 10d, Table S.1). Additionally, oxidation of the bimetal surface had increased slightly after treatment according to EDS compositional relative quantification (Table S.1). While EDS compositional analyses are generally used for smoother and flat sample surfaces (whereas the analyzed bimetal surfaces have varying topography), the compositions obtained by EDS were still considered one effective measure of overall oxidation as seen in other bimetal literature (Shih *et al.*, 2009; Xu *et al.*, 2012; Nie *et al.*, 2013). In the present study, similar results to that of EDS analyses of Mg/Cu particles were found for Mg/Ni and Mg/Zn particles; i.e. oxidation was evident to some extent on the surface of unused and was more pronounced on used particles (Table S.1; EDS elemental mappings of these particles are provided in the supplemental data, Figures S.6-S.9).

**Fig. 10** EDS mapping of (a) SEM of sample region of a used Mg/Cu particle elucidating distribution of (b) primary metal Mg to (c) oxygen, and (d) catalytic metal Cu

### 3.8.2 *Identification and Relative Quantification of Oxidized Species*

The major oxidized species was identified as $Mg(OH)_2$ through XRD analysis for all three bimetal configurations. Furthermore, MgO formation was not observed. The oxidation of the base metal Mg was consistent with galvanic corrosion when in contact with the catalytic metal (i.e. Cu, Ni or Zn).

The presence of $Mg(OH)_2$ was corroborated on the surface of all three unused bimetal particles, however, to a lesser extent on Mg/Ni and Mg/Zn than on Mg/Cu. The reduced formation of $Mg(OH)_2$ on Mg/Ni and Mg/Zn is in agreement with the lower galvanic potential difference for these bimetal systems compared to Mg/Cu (Figure S.10a,b-11a,b). After treatment of wastewater, the amount of $Mg(OH)_2$ on the surface of Mg/Cu increased significantly (Figure 10a,b), while the opposite trend was observed on the surface of used Mg/Ni and Mg/Zn particles. This may be due to the unknown ions in the wastewater, which may have solubilized part of the $Mg(OH)_2$ formed on the latter two bimetals. However, in the case of Mg/Cu, the formation of hydroxide from high galvanic potential difference likely exceeded the rate of $Mg(OH)_2$ dissolution due to unknown ions, therefore resulting in the expected increase of hydroxide formation. This is also supported by observations made on the bimetal surfaces after treatment of aqueous solutions of pure DNAN (i.e. a matrix lacking additional ions), where the trend in oxidation of Mg for each bimetal configuration showed the expected outcome, i.e. the amount of $Mg(OH)_2$ increased after 2.5 hours of treatment (Figures 11c, S.10c, S.11c). Further analysis on the ionic character and composition of the wastewater is required.

**Fig. 11** XRD patterns of Mg/Cu (a) before treatment, (b) after treatment in wastewater, and (c) after treatment in aqueous solutions

The decrease of $Mg(OH)_2$ on used particles of Mg/Ni and Mg/Zn may contradict the findings from EDS, which showed that overall oxygen content/oxidation increased. However, it is possible that XRD could not detect other oxidized species since XRD is a technique that detects crystalline materials.

In addition, there were unidentified species (small peaks at 33 and 43 2Θ) that were not matched to any oxidized forms of Cu or Mg with Cu. In the treatment of nitrate by Fe/Cu (Khalil *et al.*, 2016), species of Fe and Cu oxides were detected, specifically $Fe_3O_4$ and $CuFe_2O_4$•$Fe_3O_4$. However, no other oxidized species of Cu were detected in the present work. Furthermore, micron-sized deposits of $Zn^0$ were observed, likely due to their larger particle size and increased detection on XRD. $Zn^0$ was the only zero-valent catalytic metal detected in the present work.

Despite significant oxidation of the Mg surface, treatment with the Mg-bimetals produced high removals of DNAN. During treatment with ZVI or Fe-bimetals, the formation of (oxy)hydroxides or oxides of iron passivate the surface causing inhibition of treatment (Fu, Cheng and Lu, 2015; Sun *et al.*, 2016). In the treatment with various Fe-bimetal configurations, the passivated Fe-bimetals led to separate modelling of a slower kinetics and "inhibited" reaction rate after an initial period of faster kinetics (Rivero-Huguet and Marshall, 2009). Generally, a low pH condition for various Fe-based bimetals have been required in order to overcome passivation by oxidation (Xu *et al.*, 2005; Rivero-Huguet and Marshall, 2009; Luo *et al.*, 2010). However, in the present work, an unadjusted pH condition (Table 2) in each bimetal treatment system still produced effective DNAN removal.

## 4. Conclusions

The preliminary work performed in this study indicates that Mg-based bimetals are effective reagents for the degradation of DNAN and other energetic compounds often present in munitions facilities waste streams. The use of inexpensive catalytic metals to generate effective Mg-bimetal reagents was demonstrated by the high removals of DNAN, TOC and COD. Oxidation of the Mg-bimetal surface did not inhibit the treatment, as opposed to oxidation on ZVI or Fe-bimetals passivating the surface and inhibiting treatment. Future work may be performed on the impact of

537 catalytic metal dose relative to the base metal and the coating method during bimetal synthesis.
538 These parameters subsequently may be correlated to overall removals and removal kinetics. In
539 addition, the reaction occurred at neutral to basic pH, i.e. without the need to lower the pH of the
540 treated solution as is commonly the case with Fe-based bimetals. This eliminates the need for an
541 additional chemical in a treatment scenario. Byproduct identification and subsequent
542 determination of the reaction pathways demonstrated that DNAN was reduced to amino
543 derivatives 2-ANAN, 4-ANAN and subsequently to DAAN. The 91% closure for the carbon
544 mass balance indicated that the dissolved and adsorbed phases contained 12.4% and 78.4% TOC,
545 respectively. The significant carbon adsorbed to the Mg-bimetal surface requires further
546 investigation in either the extraction of these adsorbed compounds or direct analysis of used Mg-
547 bimetal particles. In both the dissolved and adsorbed phases, after complete product
548 identification, closure of the mass balance should be obtained. Furthermore, the proposed end-
549 product DAAN requires additional confirmation (i.e. evidence that further treatment of DAAN
550 does not form another compound).
551

552 **Acknowledgements**

553 This work was supported by the Consortium for Energy, Environment and Demilitarization
554 (CEED) contract number SINIT-15-0013. Electrospray ionization mass spectra were obtained in
555 the Center for Mass Spectrometry of Department of Chemistry and Chemical Biology of Stevens
556 Institute of Technology.
557

558 **References**

559 Agarwal, S. *et al.* (2009) 'Reactivity of substituted chlorines and ensuing dechlorination
560 pathways of select PCB congeners with Pd/Mg bimetallics', *Environmental Science and*

*Technology*, 43(3), pp. 915–921. doi: 10.1021/es802538d.

Agarwal, S., Al-Abed, S. R. and Dionysiou, D. D. (2007) 'Enhanced corrosion-based Pd/Mg bimetallic systems for dechlorination of PCBs', *Environmental Science and Technology*, 41(10), pp. 3722–3727. doi: 10.1021/es062886y.

Agarwal, S., Al-Abed, S. R. and Dionysiou, D. D. (2009) 'Impact of organic solvents and common anions on 2-chlorobiphenyl dechlorination kinetics with Pd/Mg', *Applied Catalysis B: Environmental*, 92(1–2), pp. 17–22. doi: 10.1016/j.apcatb.2009.07.029.

Aginhotri, P., Mahidrakar, A. B. and Gautam, S. K. (2011) 'Complete dechlorination of endosulfan and lindane using Mg0/Pd+4 bimetallic system', *Water Environ. Res.*, 83(September), pp. 865–873. doi: 10.2175/106143011X12928814445096.

Ahn, S. C. *et al.* (2011) 'Detoxification of PAX-21 ammunitions wastewater by zero-valent iron for microbial reduction of perchlorate', *Journal of Hazardous Materials*, 192(2), pp. 909–914. doi: 10.1016/j.jhazmat.2011.05.104.

Arthur, J. D. *et al.* (2017) 'Batch soil adsorption and column transport studies of 2,4-dinitroanisole (DNAN) in soils', *Journal of Contaminant Hydrology*, 199, pp. 14–23. doi: 10.1016/j.jconhyd.2017.02.004.

Asgari, G., Ramavandi, B. and Farjadfard, S. (2013) 'Abatement of Azo Dye from Wastewater Using Bimetal-Chitosan', 2013.

Begum, A. and Gautam, S. K. (2011) 'Dechlorination of endocrine disrupting chemicals using $Mg^0/ZnCl_2$ bimetallic system', *Water Research*. Elsevier Ltd, 45(7), pp. 2383–2391. doi: 10.1016/j.watres.2011.01.017.

Coutts, J. L. *et al.* (2011) 'The use of mechanical alloying for the preparation of palladized magnesium bimetallic particles for the remediation of PCBs', *Journal of Hazardous Materials*.

584 Elsevier B.V., 192(3), pp. 1380–1387. doi: 10.1016/j.jhazmat.2011.06.052.
585 Cwiertny, D. M. *et al.* (2006) 'Exploring the influence of granular iron additives on 1,1,1-
586 trichloroethane reduction', *Environmental Science and Technology*, 40(21), pp. 6837–6843. doi:
587 10.1021/es060921v.
588 DeVor, R. *et al.* (2008) 'Dechlorination comparison of mono-substituted PCBs with Mg/Pd in
589 different solvent systems', *Chemosphere*, 73(6), pp. 896–900. doi:
590 10.1016/j.chemosphere.2008.07.006.
591 DeVor, R. *et al.* (2009) 'Mechanism of the degradation of individual PCB congeners using
592 mechanically alloyed Mg/Pd in methanol', *Chemosphere*. Elsevier Ltd, 76(6), pp. 761–766. doi:
593 10.1016/j.chemosphere.2009.05.007.
594 Fida, T. T. *et al.* (2014) 'Aerobic biodegradation of 2,4-dinitroanisole by Nocardioides sp. strain
595 JS1661', *Applied and Environmental Microbiology*, 80(24), pp. 7725–7731. doi:
596 10.1128/AEM.02752-14.
597 Fu, F., Cheng, Z. and Lu, J. (2015) 'Synthesis and use of bimetals and bimetal oxides in
598 contaminants removal from water: a review', *RSC Adv.*, 5(104), pp. 85395–85409. doi:
599 10.1039/C5RA13067K.
600 Gautam, S. K. and Suresh, S. (2007) 'Complete dechlorination of DDE/DDD using
601 magnesium/palladium system', *Water Environment Research*, 79(Ddd), pp. 430–435. doi:
602 10.2175/106143006x115336.
603 Ghauch, A. and Tuqan, A. (2009) 'Reductive destruction and decontamination of aqueous
604 solutions of chlorinated antimicrobial agent using bimetallic systems', *Journal of Hazardous
605 Materials*, 164(2–3), pp. 665–674. doi: 10.1016/j.jhazmat.2008.08.048.
606 Hadnagy, E., Rauch, L. M. and Gardner, K. H. (2007) 'Dechlorination of polychlorinated

biphenyls, naphthalenes and dibenzo-p-dioxins by magnesium/palladium bimetallic particles.', *Journal of environmental science and health. Part A, Toxic/hazardous substances & environmental engineering*, 42(6), pp. 685–695. doi: 10.1080/10934520701326222.

Hawari, J. *et al.* (2015) 'Environmental fate of 2,4-dinitroanisole (DNAN) and its reduced products', *Chemosphere*. Elsevier Ltd, 119, pp. 16–23. doi: 10.1016/j.chemosphere.2014.05.047.

Hudlicky, M. (Virginia P. I. and S. U. (1984) *Reductions in Organic Chemistry - Hudlicky M..pdf*. John Wiley & Sons.

Ileri, B., Ayyildiz, O. and Apaydin, O. (2015) 'Ultrasound-assisted activation of zero-valent magnesium for nitrate denitrification: Identification of reaction by-products and pathways', *Journal of Hazardous Materials*, 292(3), pp. 1–8. doi: 10.1016/j.jhazmat.2015.03.004.

Karthikeyan, S. and Spain, J. C. (2016) 'Biodegradation of 2,4-dinitroanisole (DNAN) by Nocardioides sp. JS1661 in water, soil and bioreactors', *Journal of Hazardous Materials*. Elsevier B.V., 312, pp. 37–44. doi: 10.1016/j.jhazmat.2016.03.029.

Khalil, A. M. E. *et al.* (2016) 'Promoting nitrate reduction kinetics by nanoscale zero valent iron in water via copper salt addition', *Chemical Engineering Journal*. Elsevier B.V., 287, pp. 367–380. doi: 10.1016/j.cej.2015.11.038.

Kitcher, E. *et al.* (2017) 'Characteristics and products of the reductive degradation of 3-nitro-1,2,4-triazol-5-one (NTO) and 2,4-dinitroanisole (DNAN) in a Fe-Cu bimetal system', *Environmental Science and Pollution Research*, 24(3), pp. 2744–2753. doi: 10.1007/s11356-016-8053-7.

Koutsospyros, A. *et al.* (2012) 'Degradation of high energetic and insensitive munitions compounds by Fe/Cu bimetal reduction', *Journal of Hazardous Materials*. Elsevier B.V., 219–220, pp. 75–81. doi: 10.1016/j.jhazmat.2012.03.048.

630 Lee, G. and Park, J. (2013) 'Reaction of zero-valent magnesium with water: Potential
631 applications in environmental remediation', *Geochimica et Cosmochimica Acta*. Elsevier Ltd,
632 102, pp. 162–174. doi: 10.1016/j.gca.2012.10.031.
633 Liu, J. *et al.* (2015) 'Selective removal of nitroaromatic compounds from wastewater in an
634 integrated zero valent iron (ZVI) reduction and ZVI/H2O2 oxidation process', *RSC Advances*.
635 Royal Society of Chemistry, 5, pp. 57444–57452. doi: 10.1039/C5RA08487C.
636 Luo, S. *et al.* (2010) 'Reductive degradation of tetrabromobisphenol A over iron-silver bimetallic
637 nanoparticles under ultrasound radiation', *Chemosphere*. Elsevier Ltd, 79(6), pp. 672–678. doi:
638 10.1016/j.chemosphere.2010.02.011.
639 Morales, J. *et al.* (2002) 'Hydrogenation of Phenol by the Pd/Mg and Pd/Fe Bimetallic Systems
640 under Mild Reaction Conditions', *Industrial & Engineering Chemistry Research*, 41(13), pp.
641 3071–3074. doi: 10.1021/ie0200510.
642 Nie, X. *et al.* (2013) 'Rapid degradation of hexachlorobenzene by micron Ag/Fe bimetal
643 particles', *Journal of Environmental Sciences (China)*. The Research Centre for Eco-
644 Environmental Sciences, Chinese Academy of Sciences, 25(3), pp. 473–478. doi:
645 10.1016/S1001-0742(12)60088-6.
646 Patel, U. D. and Suresh, S. (2007) 'Dechlorination of chlorophenols using magnesium-palladium
647 bimetallic system', *Journal of Hazardous Materials*, 147(1–2), pp. 431–438. doi:
648 10.1016/j.jhazmat.2007.01.029.
649 Patel, U. D. and Suresh, S. (2008) 'Effects of solvent, pH, salts and resin fatty acids on the
650 dechlorination of pentachlorophenol using magnesium-silver and magnesium-palladium
651 bimetallic systems', *Journal of Hazardous Materials*, 156(1–3), pp. 308–316. doi:
652 10.1016/j.jhazmat.2007.12.021.

653 Ramavandi, B. *et al.* (2011) 'Experimental investigation of the chemical reduction of nitrate ion
654 in aqueous solution by Mg/Cu bimetallic particles', *Reaction Kinetics, Mechanisms and*
655 *Catalysis*, 102(2), pp. 313–329. doi: 10.1007/s11144-010-0274-z.
656 Rao, B. *et al.* (2013a) 'Photochemical transformation of the insensitive munitions compound 2,4-
657 dinitroanisole', *Science of the Total Environment*, 443, pp. 692–699. doi:
658 10.1016/j.scitotenv.2012.11.033.
659 Rao, B. *et al.* (2013b) 'Photochemical transformation of the insensitive munitions compound 2,4-
660 dinitroanisole', *Science of the Total Environment*. Elsevier B.V., 443, pp. 692–699. doi:
661 10.1016/j.scitotenv.2012.11.033.
662 Rivero-Huguet, M. and Marshall, W. D. (2009) 'Reduction of hexavalent chromium mediated by
663 micro- and nano-sized mixed metallic particles', *Journal of Hazardous Materials*, 169(1–3), pp.
664 1081–1087. doi: 10.1016/j.jhazmat.2009.04.062.
665 Saitta, E. K. H. *et al.* (2015) 'Case study of a non-destructive treatment method for the
666 remediation of military structures containing polychlorinated biphenyl contaminated paint',
667 *Journal of Environmental Management*. Elsevier Ltd, 158, pp. 40–47. doi:
668 10.1016/j.jenvman.2015.04.038.
669 Shen, J. *et al.* (2013) 'Pretreatment of 2 , 4-dinitroanisole ( DNAN ) producing wastewater using
670 a combined zero-valent iron ( ZVI ) reduction and Fenton oxidation process', *Journal of*
671 *Hazardous Materials*, 260, pp. 993–1000. doi: 10.1016/j.jhazmat.2013.07.003.
672 Shih, Y. hsin *et al.* (2009) 'Dechlorination of hexachlorobenzene by using nanoscale Fe and
673 nanoscale Pd/Fe bimetallic particles', *Colloids and Surfaces A: Physicochemical and*
674 *Engineering Aspects*, 332(2–3), pp. 84–89. doi: 10.1016/j.colsurfa.2008.09.031.
675 Solanki, J. N. and Murthy, Z. V. P. (2011) 'Reduction of 4-chlorophenol by Mg and Mg-Ag

676 bimetallic nanocatalysts', *Industrial and Engineering Chemistry Research*, 50(24), pp. 14211–
677 14216. doi: 10.1021/ie2022338.
678 Sun, Y. *et al.* (2016) 'The influences of iron characteristics, operating conditions and solution
679 chemistry on contaminants removal by zero-valent iron: A review', *Water Research*, 100, pp.
680 277–295. doi: 10.1016/j.watres.2016.05.031.
681 Taylor, S. *et al.* (2017) 'Photo-degradation of 2,4-dinitroanisole (DNAN): An emerging
682 munitions compound', *Chemosphere*, 167, pp. 193–203. doi:
683 10.1016/j.chemosphere.2016.09.142.
684 Xiong, Z. *et al.* (2015) 'Comparative study on the reactivity of Fe/Cu bimetallic particles and
685 zero valent iron (ZVI) under different conditions of N<inf>2</inf>, air or without aeration',
686 *Journal of Hazardous Materials*. Elsevier B.V., 297, pp. 261–268. doi:
687 10.1016/j.jhazmat.2015.05.006.
688 Xu, F. *et al.* (2012) 'Highly active and stable Ni-Fe bimetal prepared by ball milling for catalytic
689 hydrodechlorination of 4-chlorophenol', *Environmental Science and Technology*, 46(8), pp.
690 4576–4582. doi: 10.1021/es203876e.
691 Xu, X. *et al.* (2005) 'Catalytic dechlorination kinetics of p-dichlorobenzene over Pd/Fe
692 catalysts', *Chemosphere*, 58(8), pp. 1135–1140. doi: 10.1016/j.chemosphere.2004.07.010.

693

694

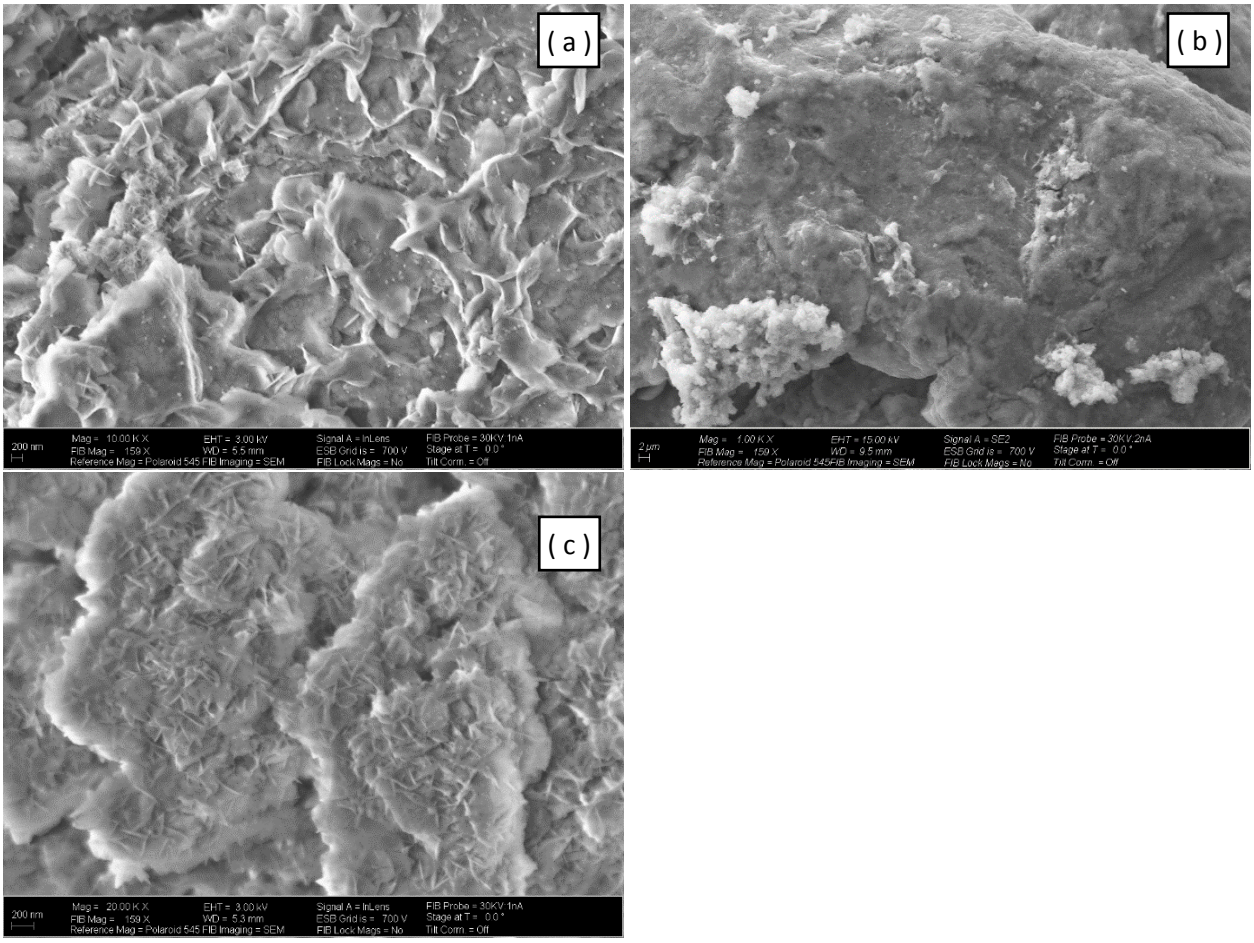


695

696

697

698 Fig 1

699 Images output by SEM Analysis.

700

701

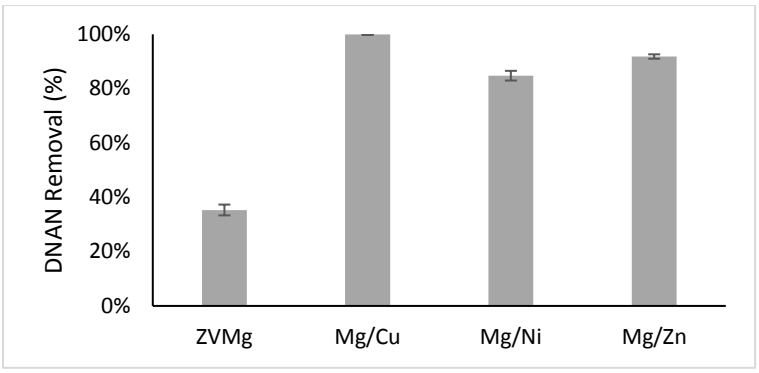


Fig 2

Created on Microsoft Excel.

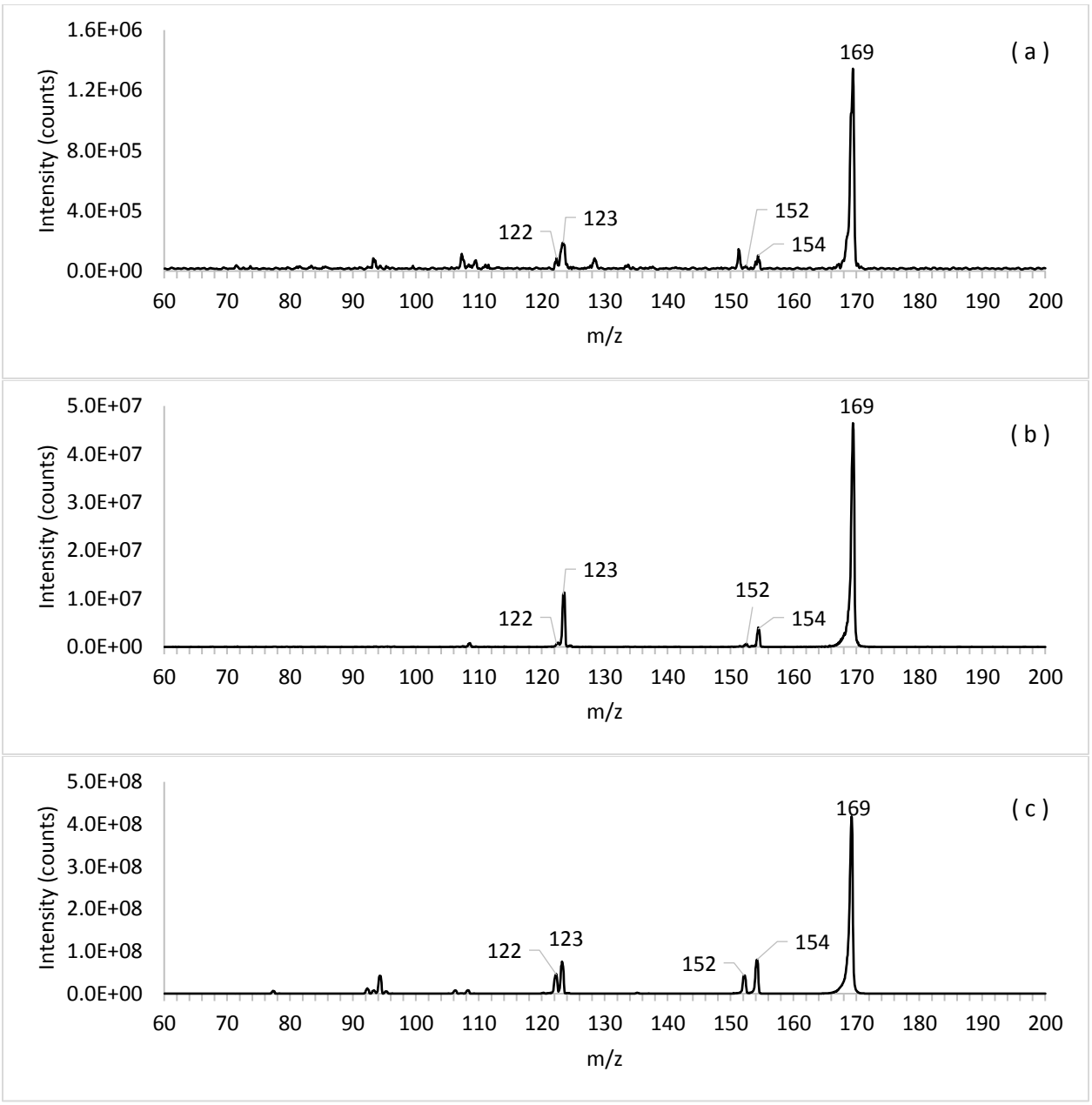


Fig 3

Figure generated by Microsoft Excel.

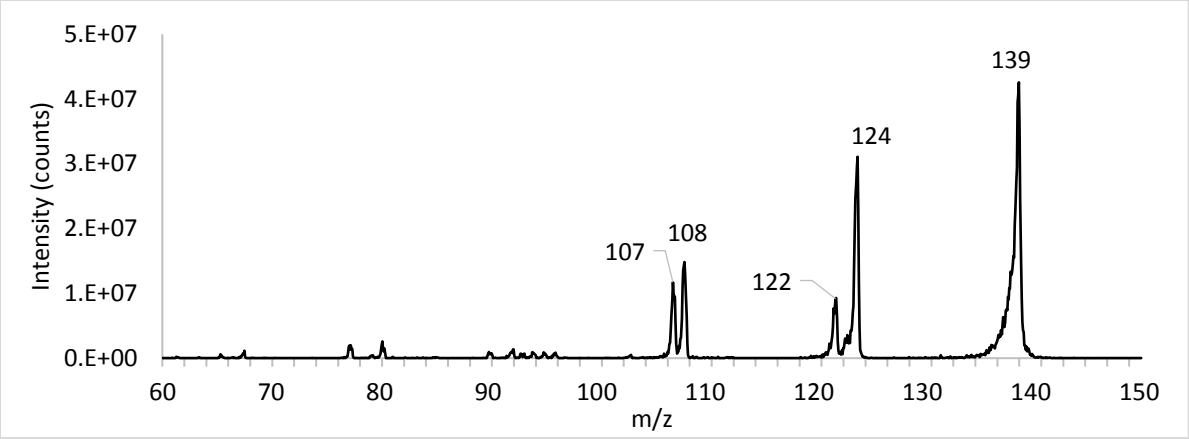


716

717 Fig 4

718 Figure generated by Microsoft Excel.

719

720

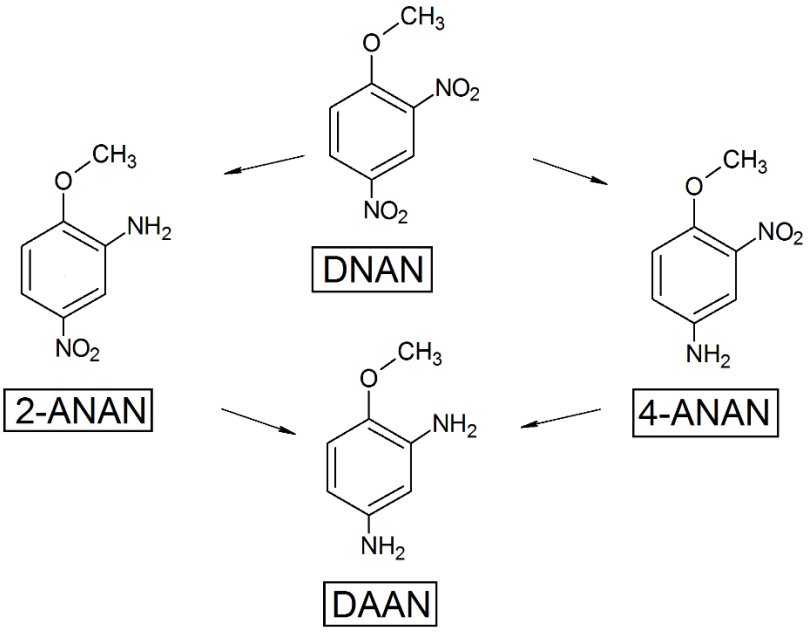


721

722

723 Fig 5

724 Figure generated by ChemCad Free Version.

725

726

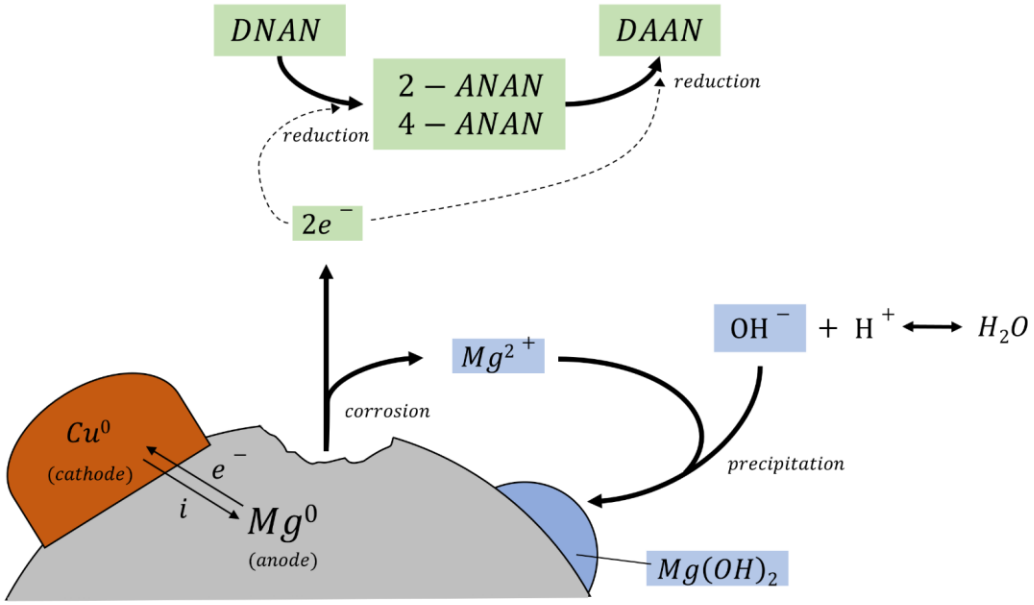


727

728 Fig 6

729 Generated on Microsoft Powerpoint

730

731

732

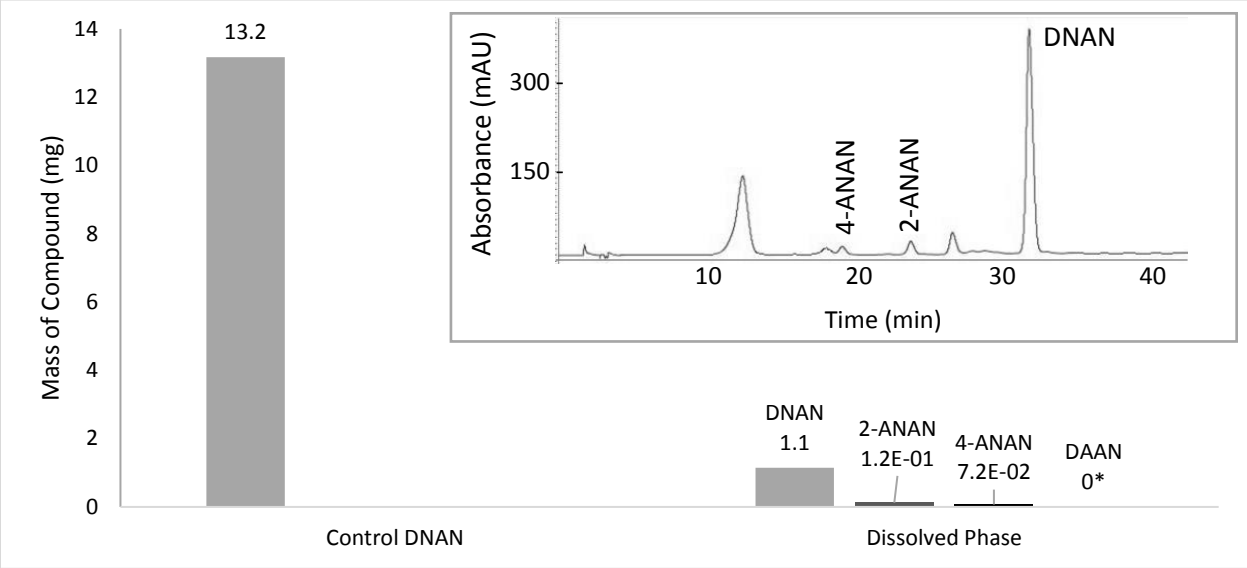


733
734

735 Fig 7

736 Figure generated by Microsoft Excel and Word.

737

738

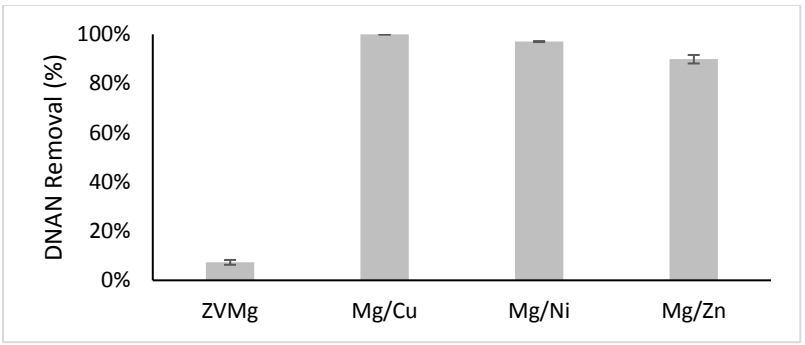


739

740 Fig 8

741 Created on Microsoft Excel.

742

743

744

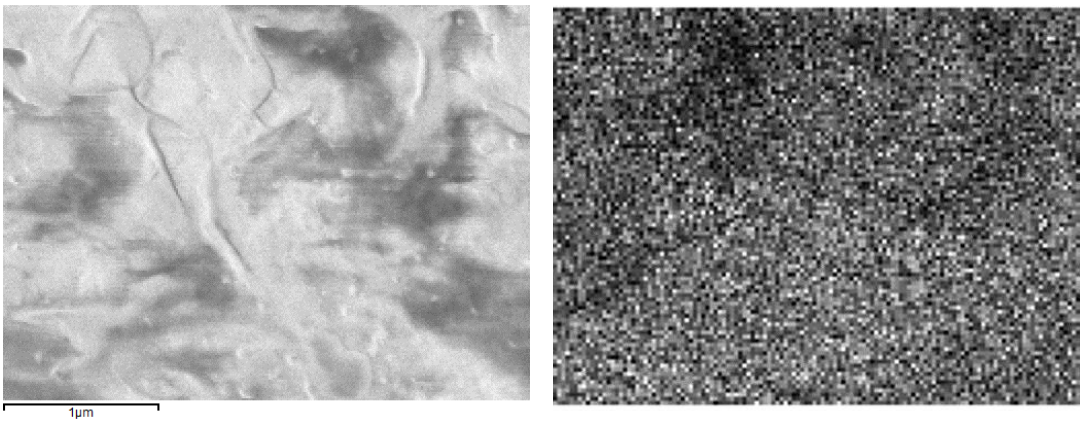


SEM: Mg/Cu ( a ) Mg ( b )

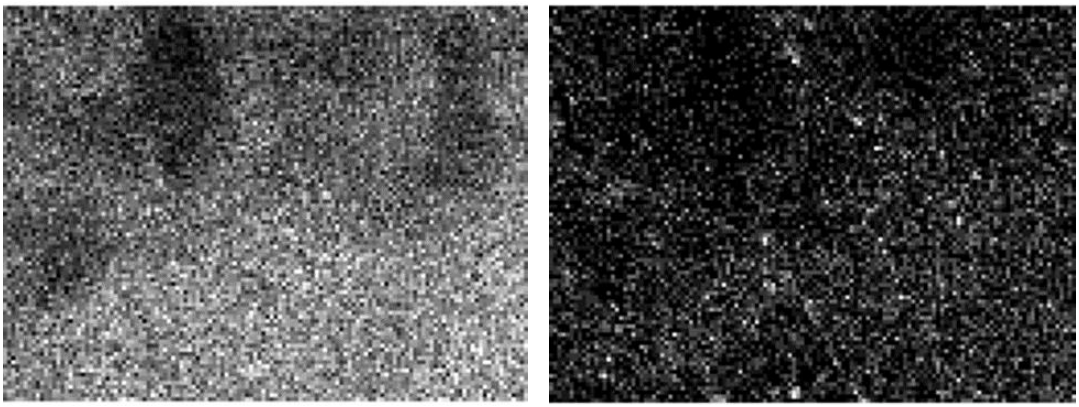

O ( c ) Cu ( d )

Fig 9

Images generated by EDS mapping.

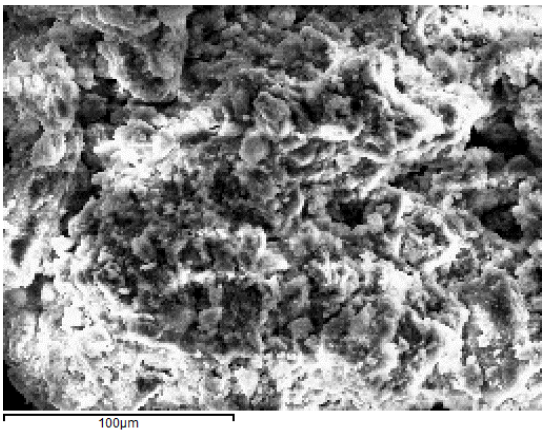


SEM: Mg/Cu ( a )

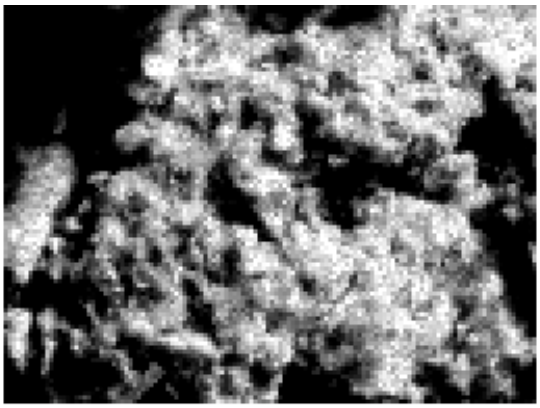

Mg ( b )

751

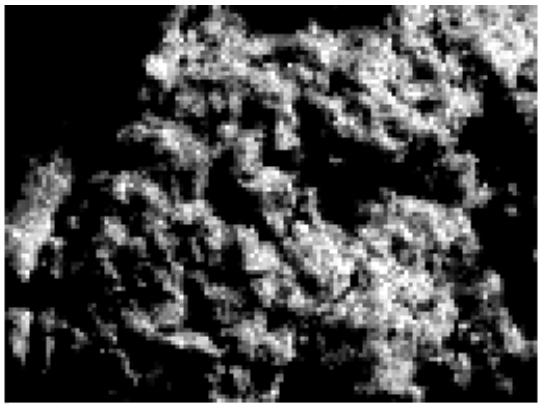

O ( c )

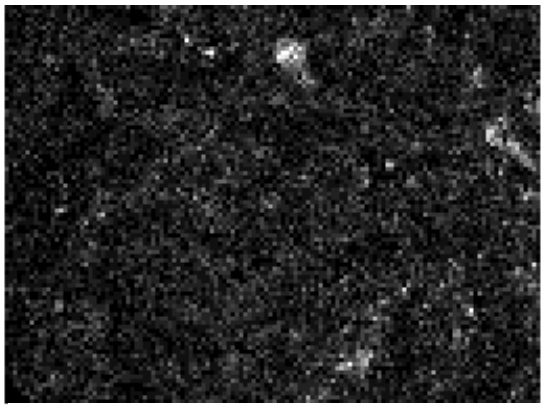

Cu ( d )

752

753 Fig 10

754 Images generated by EDS mapping.

755

756

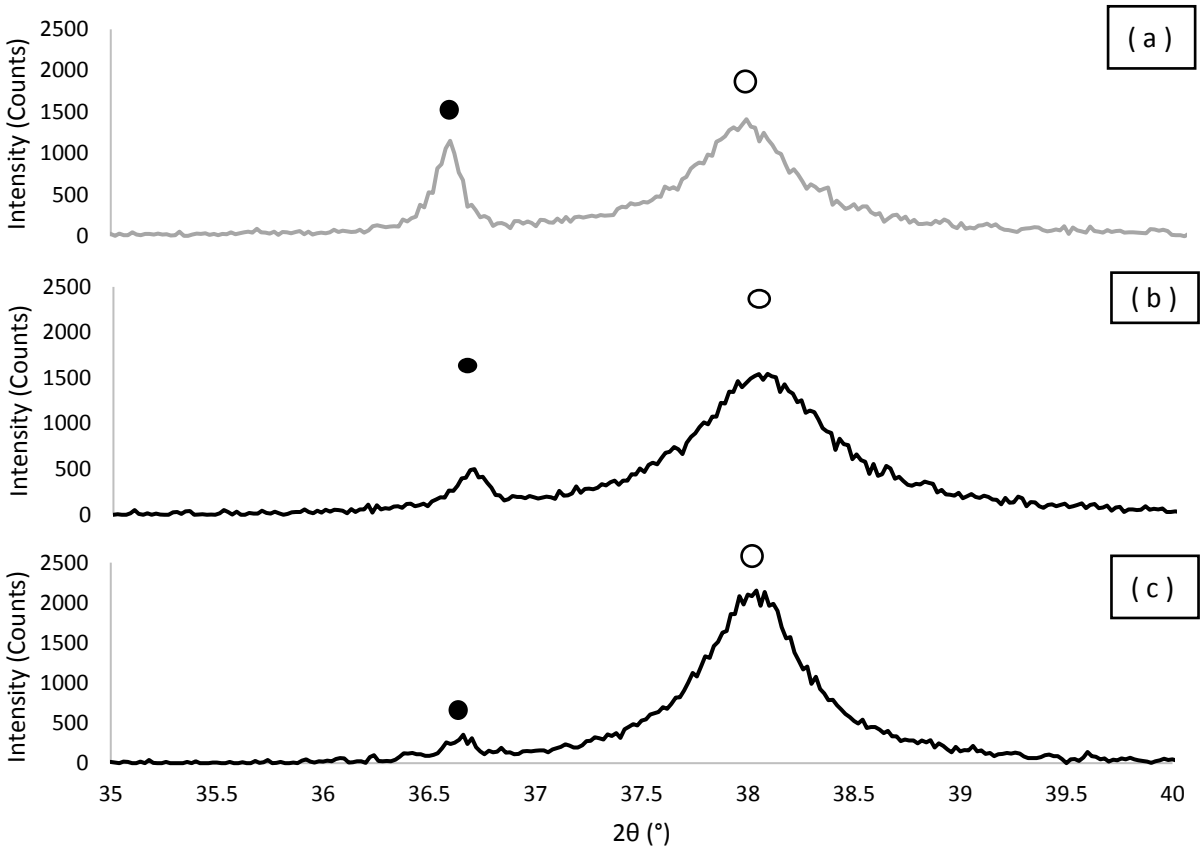


Fig 11

Figure generated by Microsoft Excel.

**Supplemental Information**

# Characterization of Mg-based Bimetal Treatment of Insensitive Munition 2,4-dinitroanisole

Emese Hadnagy[1,*], Andrew Mai[2], Benjamin Smolinski[3], Washington Braida[2], Agamemnon Koutsospyros[1]

**Submitted to:**

Environmental Science and Pollution Research

[*]Corresponding Author. *Email address:* EHadnagy@newhaven.edu
[1]Department of Civil and Environmental Engineering, University of New Haven
[2]Department of Civil, Environmental, and Ocean Engineering, Stevens Institute of Technology
[3]RDECOM-ARDEC

**Table S.1** Elemental Compositions (% Mass) of Bimetal Surfaces

| Bimetal | | O | Mg | Cu, Ni or Zn |
|---|---|---|---|---|
| Mg/Cu | Unused | 53.1 | 34.7 | 12.2 |
| | Used | 65.6 | 34.4 | 0.6 |
| Mg/Ni | Unused | 44.7 | 14.7 | 40.6 |
| | Used | 54.4 | 18.8 | 26.8 |
| Mg/Zn | Unused | 41.9 | 23.4 | 34.7 |
| | Used | 53.8 | 31.5 | 14.7 |

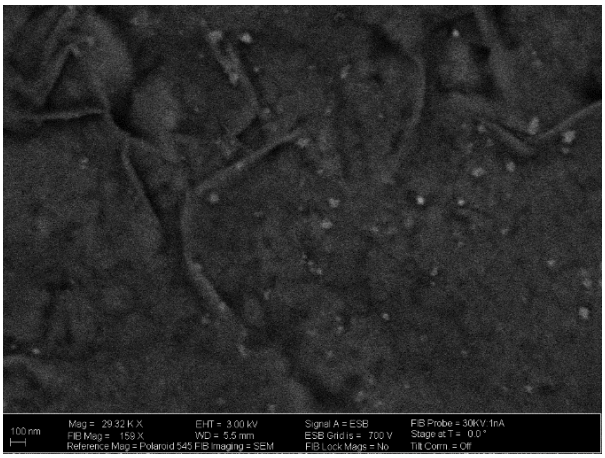


**Fig. S.1** Contrasted SEM image of sample surface of unused Mg/Cu to more easily observe Cu nanoparticles

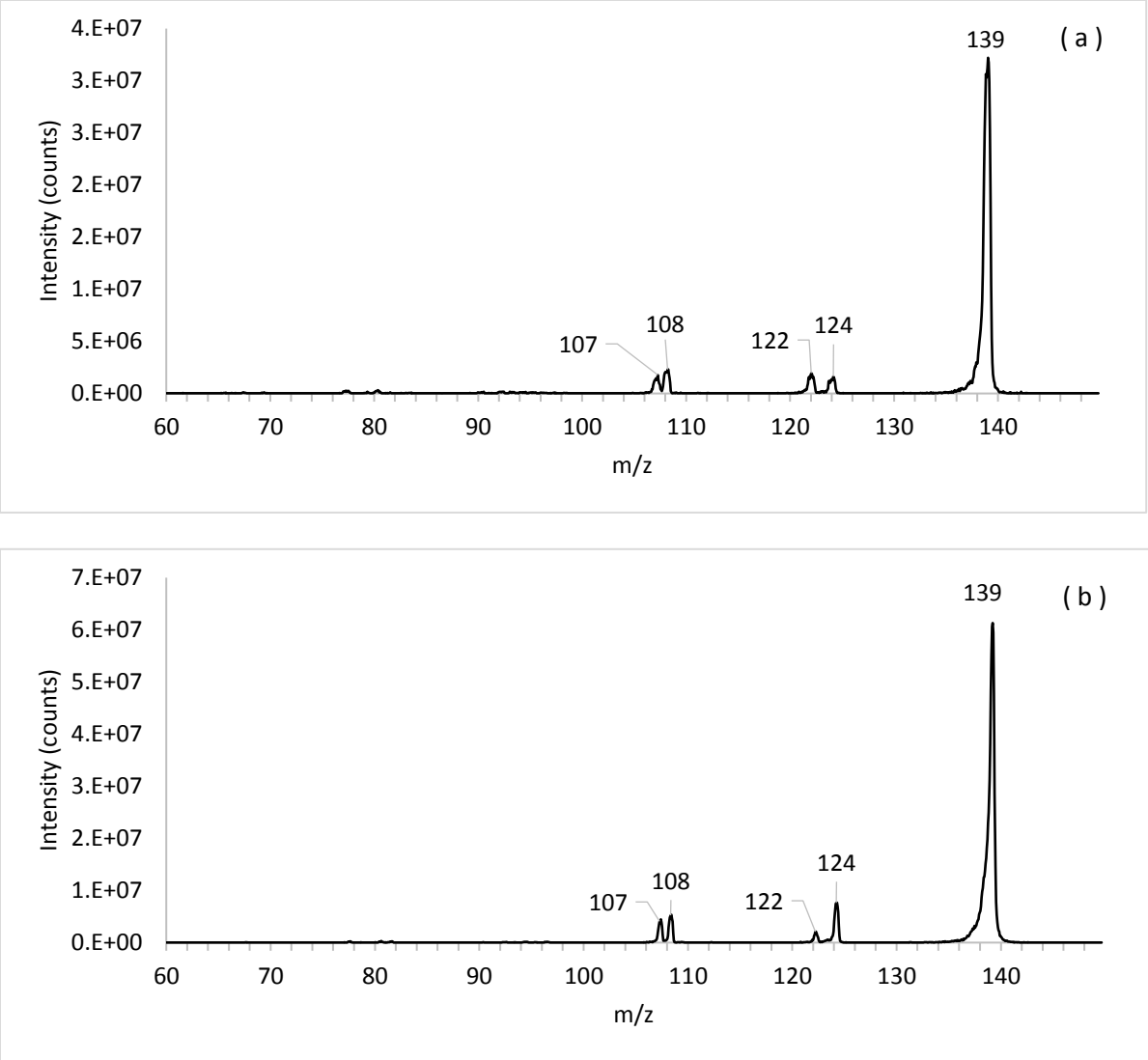


**Fig. S.2** Daughter spectrum of m/z 139 from ESI-MS/MS in positive mode from (a) after DNAN treatment (solvent matrix, 0.5% S/L, 10:1 Mg to Cu ratio and 2.5 hr treatment) and (b) pure DAAN solution reference

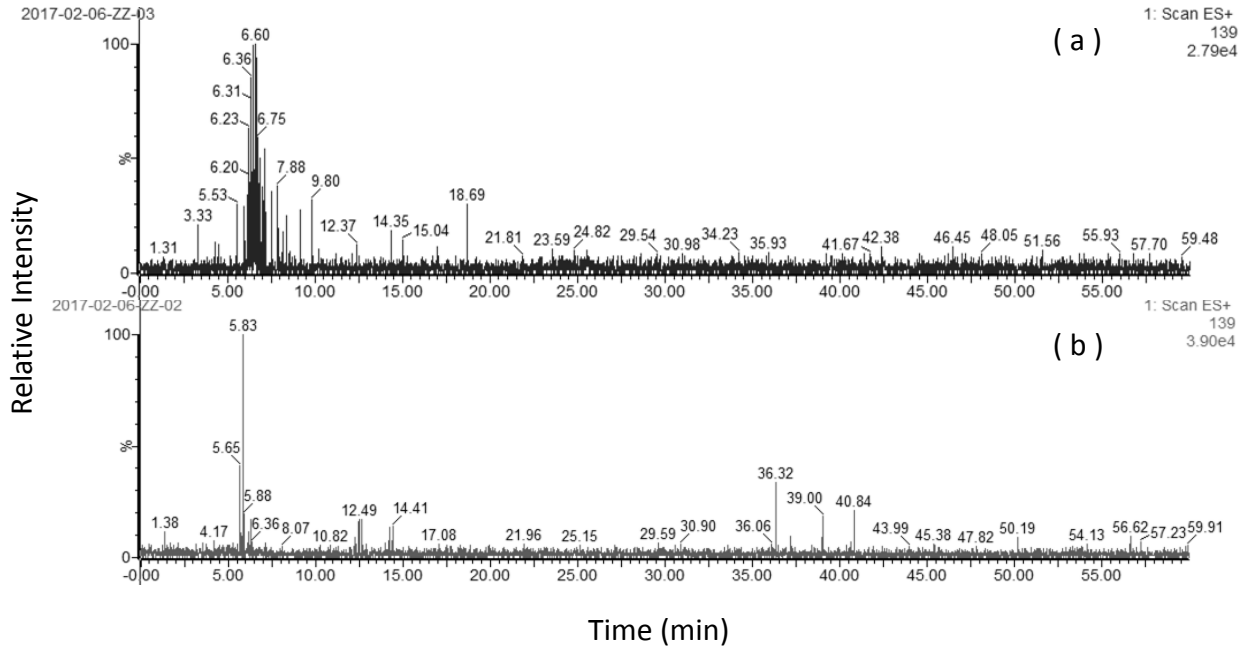


**Fig. S. 3** Mass chromatograms of selected ion m/z 139 obtained from HPLC-ESI-MS of (a) pure DAAN, and (b) treated 4-ANAN sample (aqueous solution, 0.5% S/L, 10:1 Mg to Cu ratio and 1 hr treatment) where the elution of m/z 139 was identical. The slight difference in elution times (<1min) was due to peak shifts on HPLC

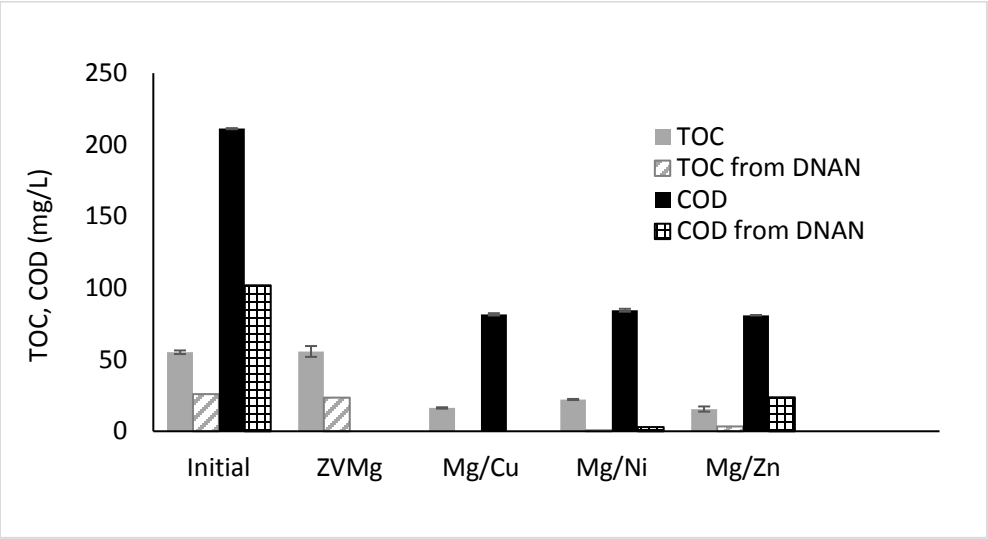


**Fig. S.4** TOC, COD (mg $L^{-1}$) and DNAN contribution to TOC and COD in treated wastewater (0.5% S/L, 10:1 Mg to catalytic metal ratio, and 2.5 h treatment time, COD not measured for ZVMg)

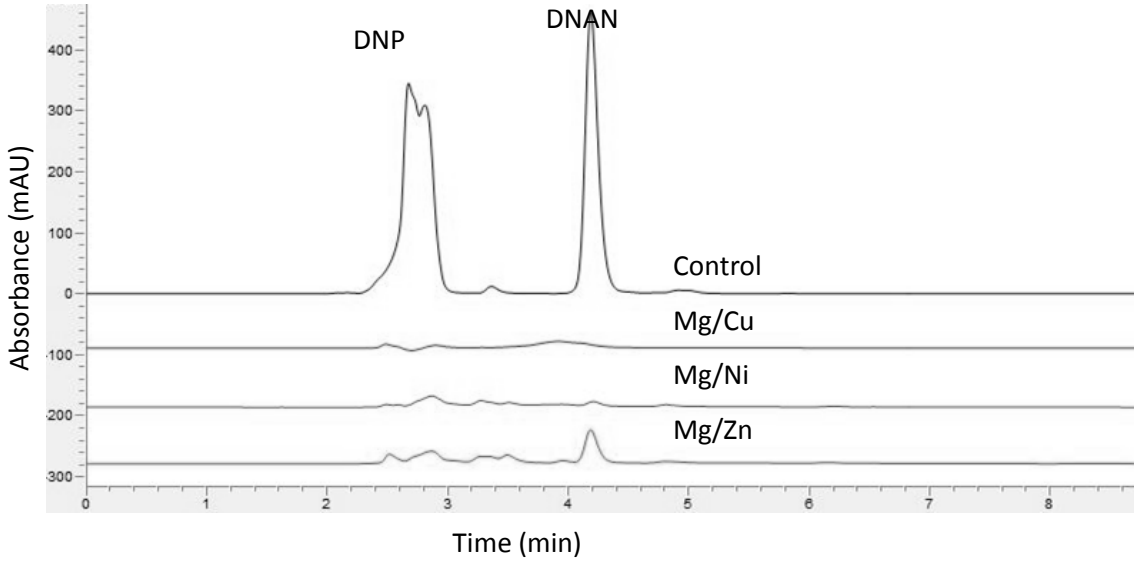


**Fig. S.5** Visualization of degradation of DNP (2.1 min) and DNAN (4.2 min) in the wastewater control (top chromatogram) versus wastewater treated with Mg/Cu, Mg/Ni and Mg/Zn using overlaid chromatograms after 150 minutes of treatment (wastewater matrix, 0.5% S/L, 10:1 Mg to secondary metal ratio)

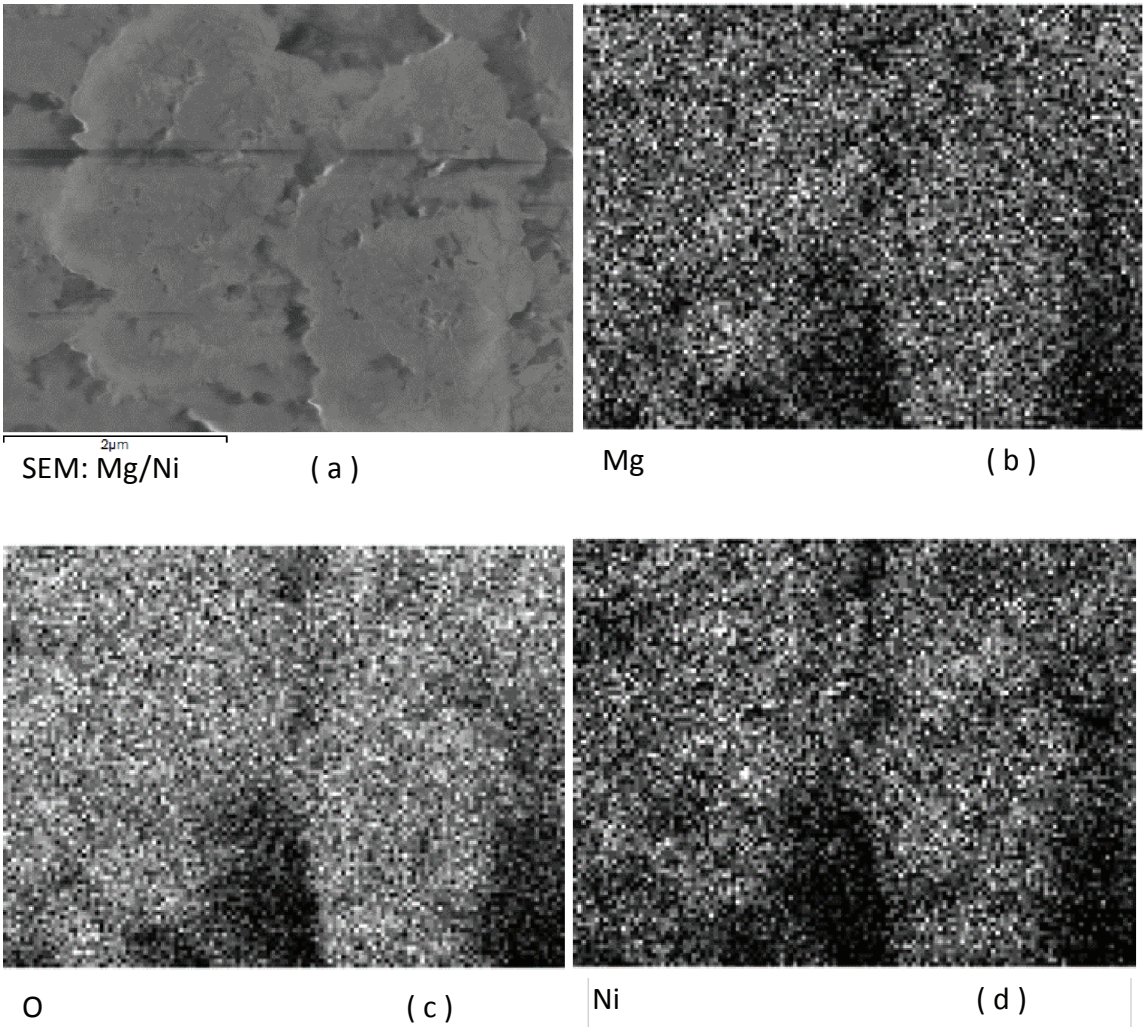


**Fig. S.6** EDS mapping of (a) sample region of an unused particle of Mg/Ni pictured by SEM elucidating distribution of (b) primary metal Mg to (c) oxygen, and (d) catalytic metal Ni

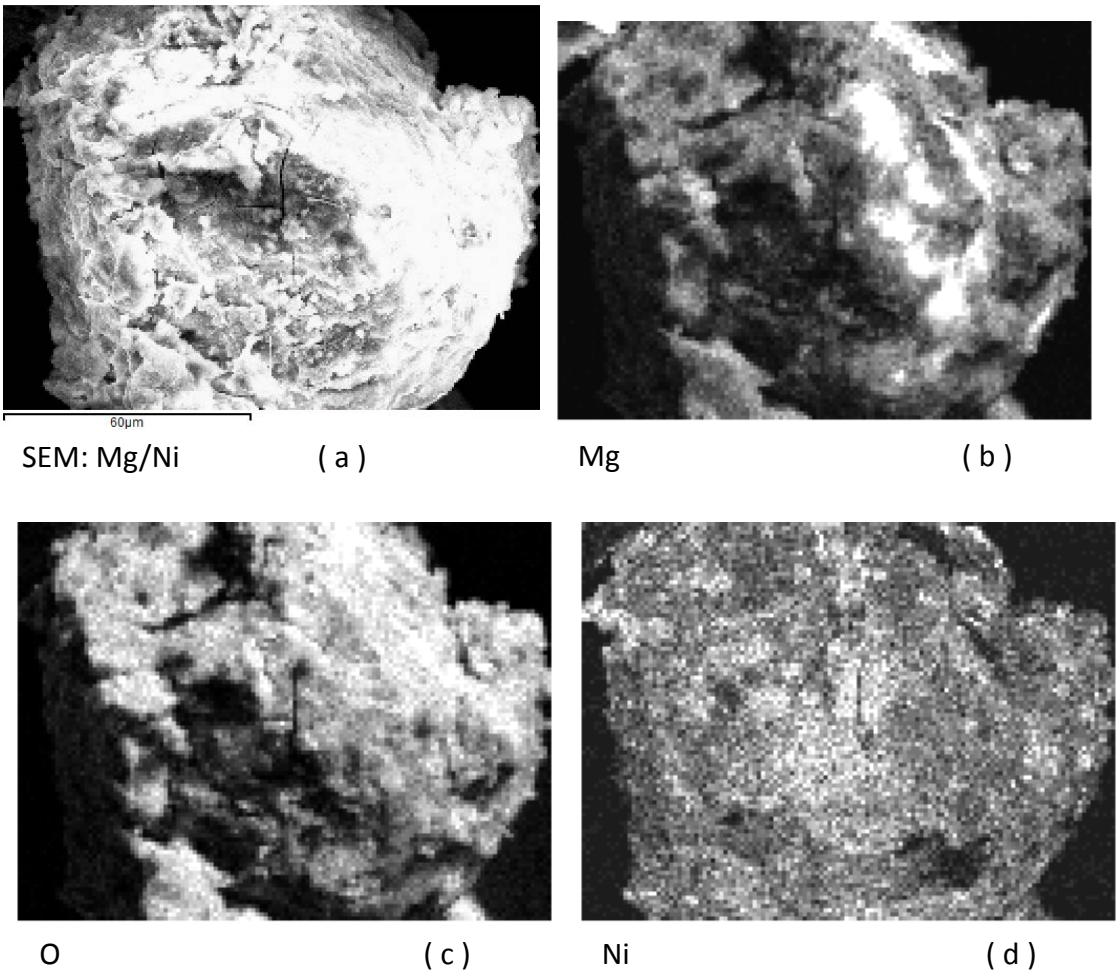


**Fig. S.7** EDS mapping of (a) sample region of a used particle of Mg/Ni pictured by SEM elucidating distribution of (b) primary metal Mg to (c) oxygen, and (d) catalytic metal Ni

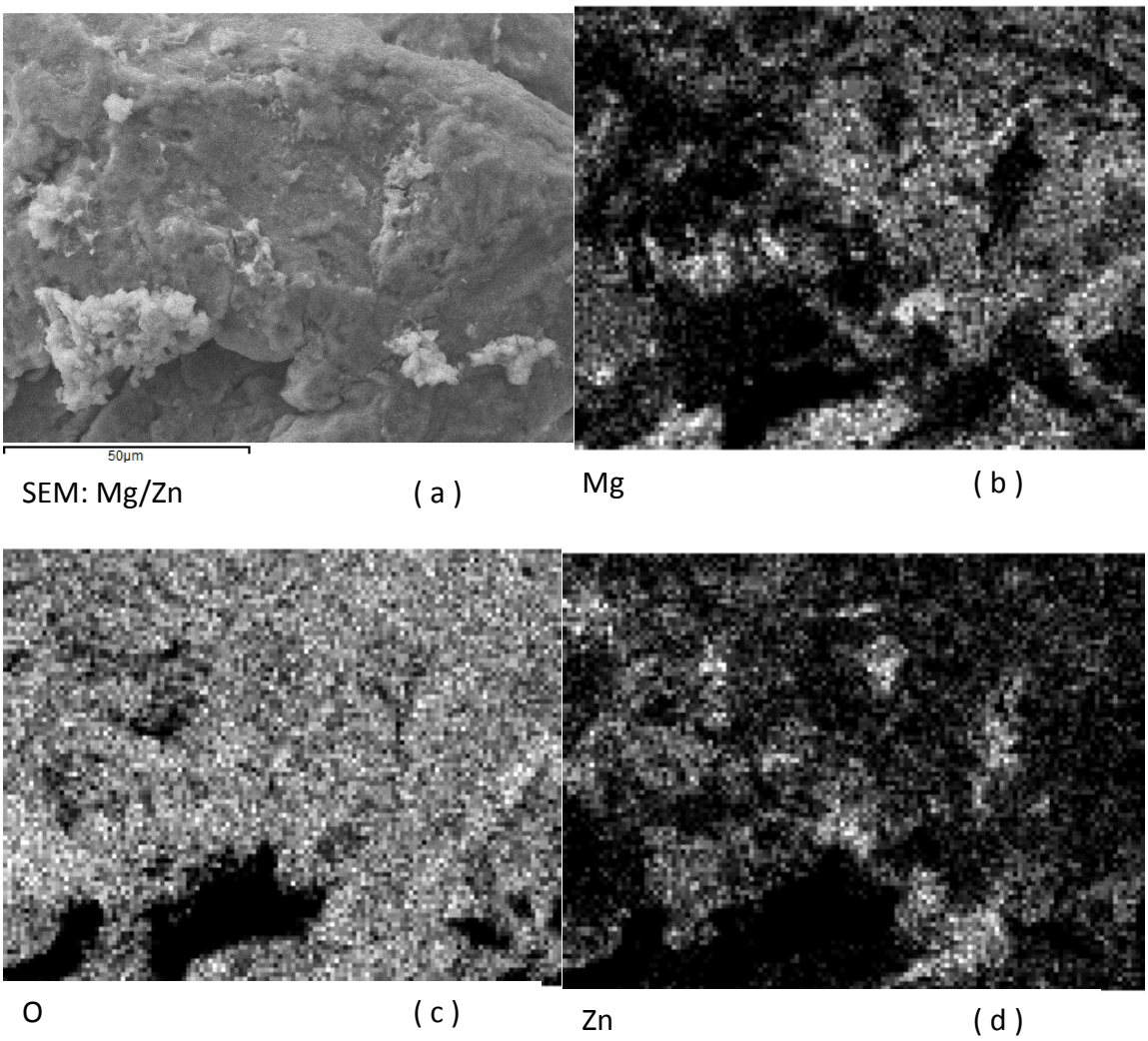


**Fig. S.8** EDS mapping of (a) sample region of an unused particle of Mg/Zn pictured by SEM elucidating distribution of (b) primary metal Mg to (c) oxygen, and (d) catalytic metal Zn

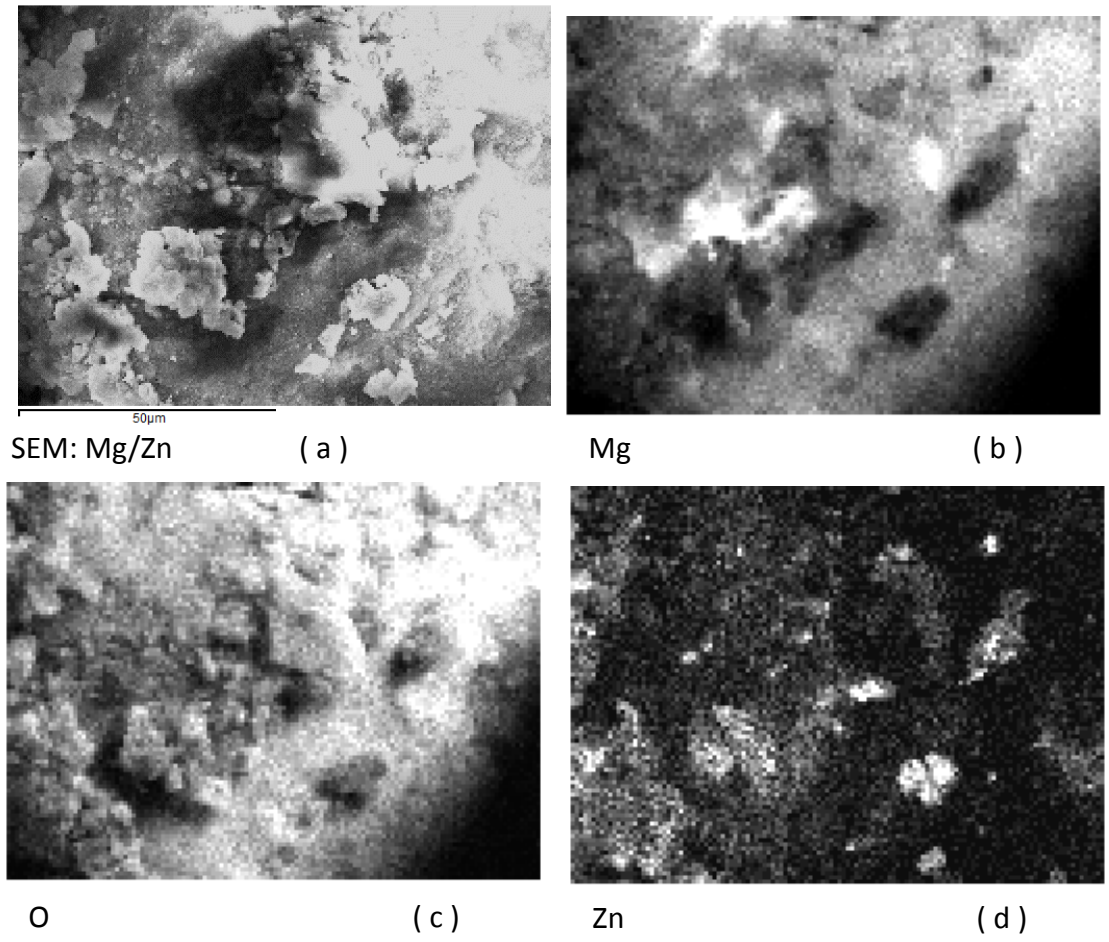


**Fig. S.9** EDS mapping of (a) sample region of a used particle of Mg/Zn pictured by SEM elucidating distribution of (b) primary metal Mg to (c) oxygen, and (d) catalytic metal Zn

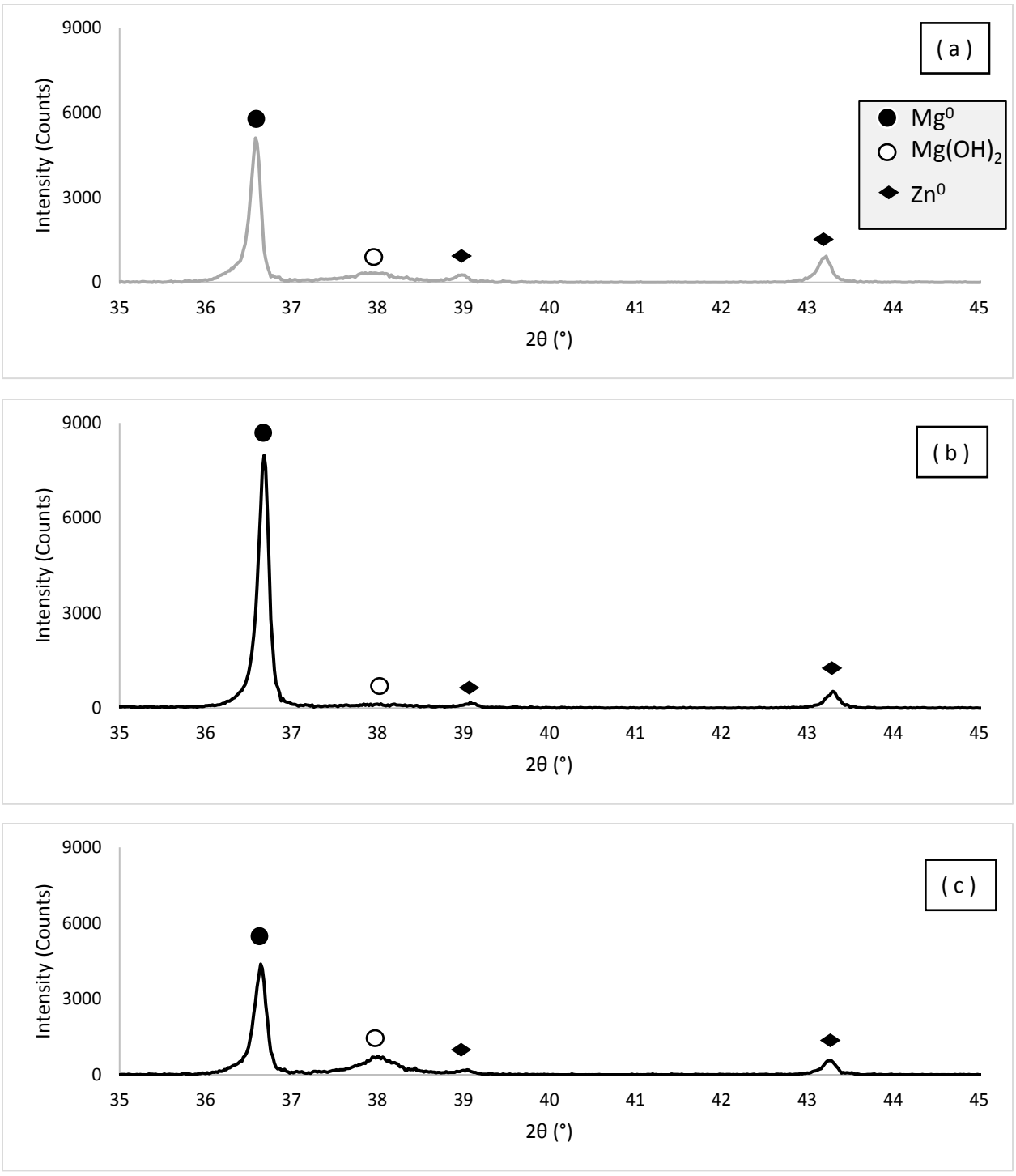


**Fig. S.10** XRD patterns of Mg/Zn (a) before treatment, (b) after treatment in wastewater, (c) and after treatment in the pure aqueous phase

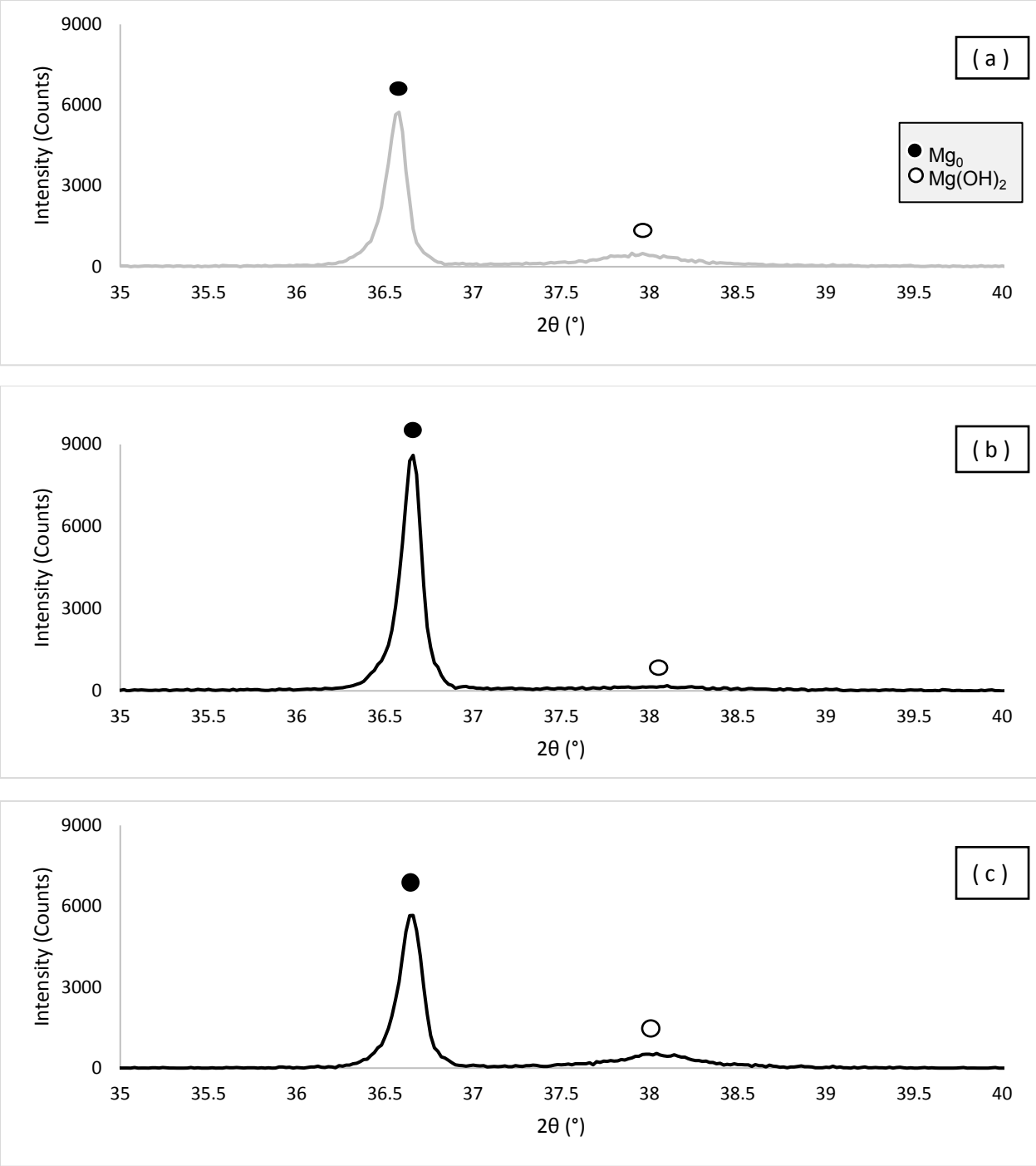


**Fig. S.11** XRD patterns of Mg/Ni (a) before treatment, (b) after treatment in wastewater, and (c) after treatment in the pure aqueous phase